uOttawa

L'Université canadienne
Canada's university

FACULTÉ DES ÉTUDES SUPÉRIEURES ET POSTOCTORALES

uOttawa

L'Université canadienne
Canada's university

FACULTY OF GRADUATE AND POSDOCTORAL STUDIES

Yu Yan

AUTEUR DE LA THÈSE / AUTHOR OF THESIS

M.A.Sc. (Electrical Engineering)

GRADE / DEGREE

Department of Electrical Engineering

FACULTÉ, ÉCOLE, DÉPARTEMENT / FACULTY, SCHOOL, DEPARTMENT

Photonic Microwave Filters with Negative and Complex Coefficients

TITRE DE LA THÈSE / TITLE OF THESIS

Prof. J. Yao

DIRECTEUR (DIRECTRICE) DE LA THÈSE / THESIS SUPERVISOR

CO-DIRECTEUR (CO-DIRECTRICE) DE LA THÈSE / THESIS CO-SUPERVISOR

EXAMINATEURS (EXAMINATRICES) DE LA THÈSE / THESIS EXAMINERS

Prof. M. Yagoub

Prof. R. Gauthier

Gary W. Slater

Le Doyen de la Faculté des études supérieures et postdoctorales / Dean of the Faculty of Graduate and Postdoctoral Studies

Photonic Microwave Filters with Negative and Complex Coefficients

By

Yu Yan

A thesis submitted in partial
fulfillment of the requirements for
the degree of

Master of Applied Science

Ottawa-Carleton Institute of Electrical and Computer Engineering
School of Information Technology and Engineering
Faculty of Engineering
University of Ottawa

September 2007

Your file Votre référence
ISBN: 978-0-494-50941-8
Our file Notre référence
ISBN: 978-0-494-50941-8

ABSTRACT

Photonic microwave filter has been a topic of interest for over two decades because of the many advantageous features such as large time-bandwidth product, wide tunability, high Q-factor, low loss, light weight, and immunity to electromagnetic interference offered by photonics.

Theoretical and experimental studies of photonic microwave filters are presented in this thesis. Three novel techniques to implement photonic microwave filters with negative coefficients and complex coefficients are proposed and experimentally demonstrated. In the first technique, the negative coefficients are generated based on cross-polarization-modulation (XPolM) in a semiconductor optical amplifier (SOA). In the second technique, negative coefficients are generated based on phase modulation and phase modulation to intensity modulation (PM-IM) conversion using linearly-chirped fiber Bragg gratings (LCFBGs) with positive and negative dispersions. In the third technique, a tunable photonic microwave filter with complex coefficients is implemented using a wideband tunable optical RF phase shifter. A technique to improve the dynamic range of a photonic microwave bandpass filter is also investigated.

TABLE OF CONTENTS

LIST OF FIGURES

Number *Page*

ACKNOWLEDGMENTS

In the first place, I would like to record my gratitude to my advisor, Professor Jianping Yao, for his supervision, advice, and guidance throughout the research work. His scientistic intuition and rich knowledge have made him as a constant source of ideas. I am very grateful for his patience, enthusiasm and encouragement.

I also would like to thank present and former members in the Microwave Photonics Research Laboratory, who are my colleagues as well as my friends: Dr. Fei Zeng, Dr. Qing Wang, Dr. Hao Chi, Sebastien Blais, Chao Wang, Honglei Guo, Howard Rideout, Dr. Yitang Dai. Their strong supports and generous help by sharing their knowledge with me greatly improved my research work.

Finally I am greatly indebted to my beloved family: my father Shourong Yan, my mother Weihong Jiao, my sister Jing Yan, and my fiancée Shiyu Gao. They have always been the biggest support to me, everywhere and everything. Their love and faith make a great environment for my study and research.

LIST OF PUBLICATIONS

Refereed journal papers:

1. Y. Yan, S. Blais, and J. P. Yao, "Tunable photonic microwave bandpass filter with negative coefficients implemented using an optical phase modulator and chirped fiber Bragg gratings," *IEEE Journal of Lightwave Technology*, vol. 25, no. 11, pp. 3283-3288, Nov. 2007.

2. Y. Yan and J. P. Yao, "A tunable photonic microwave filter with complex coefficient using an optical RF phase shifter," *IEEE Photonics Technology Letters*, vol. 19, no. 19, pp. 1472-1474, Oct. 2007.

Refereed conference papers:

3. Y. Yan and J. P. Yao, "Tunable optical microwave bandpass filter with negative coefficients based on optical phase modulator and chirped fiber Bragg gratings," oral presentation at Photonics North 2007, 95-nP7q-181, Ottawa, Canada, June 2007.

4. Y. Yan, F. Zeng, Q. Wang, and J. P. Yao, "Photonic microwave filter with negative coefficients based on cross polarization modulation in a semiconductor optical amplifier," oral presentation at OFC 2007, OWU6, Anaheim, California, USA, March 2007.

ORGANIZATION OF THE THESIS

This thesis consists of six chapters. In Chapter 1, a brief introduction to the general concepts of the transversal filters and typical structure of the photonic microwave filters are presented, followed by a review of the recently proposed approaches for the implementation of photonic microwave filters with negative and complex coefficients. Then the major contributions of this research are addressed. In Chapter 2, a photonic microwave bandpass filter with negative coefficients based on XPolM in an SOA is proposed and experimentally demonstrated. The impact of the SOA cross gain modulation (XGM) on the performance of the microwave filter is also investigated. In Chapter 3, a continuously tunable photonic microwave bandpass filter with positive and negative coefficients using an optical phase modulator and chirped FBGs is proposed and experimentally demonstrated. In Chapter 4, a novel tunable microwave filter with complex coefficients using a wideband tunable optical RF phase shifter that consists of two electro-optic intensity modulators is proposed and experimentally demonstrated. In Chapter 5, a technique to improve the dynamic range of the photonic microwave bandpass filter is discussed and experimentally investigated. Finally, a conclusion is drawn in Chapter 6 with recommendations for the future work.

Chapter 1

INTRODUCTION

Microwave signal processing in the optical domain has been a topic of interest for over two decades, thanks to the advantageous features such as broad bandwidth, low loss, light weight, and immunity to electromagnetic interference, offered by optics. Among the many microwave signal processing functionalities, microwave filtering is of particular interest. Photonic microwave filter is a system used to implement microwave filtering in the optical domain, which can provide a large tunability and a high Q factor which are usually difficult to realize through conventional electronic methods. In addition, since the microwave signal is processed directly in the optical domain without additional optical-electrical and electrical-optical conversions, the photonic microwave filters are particularly suitable for applications such as optically controlled phased-array antennas, radio-over-fiber (RoF) systems, and other microwave-photonic links (MPLs). For these reasons, photonic microwave filters have attracted considerable interest for a few years.

In this chapter, we will first introduce the general concepts of delay-line transversal filters and the typical structure of photonic microwave filters. A

review on the recent approaches proposed to implementing photonic microwave filters with negative and complex coefficients is then presented. The major contributions and organization of this thesis will be addressed in Sections 1.3 and 1.4.

1.1 General Concepts

1. 1. 1 Delay-line transversal filters

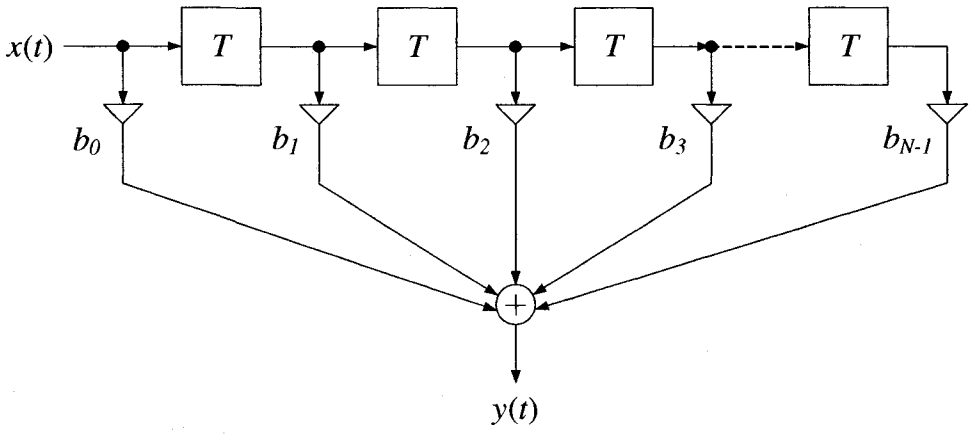

Fig. 1.1. FIR filter structure

Finite impulse response (FIR) filters can be designed to have linear phase in the whole frequency range, and are always stable with Bounded Input Bounded Output (BIBO) [1-3]. As a result, the FIR filters are often highly preferred for many applications. In this thesis, the effort is placed on the FIR

filters with bandpass functionality. Note that an FIR filter is also called a transversal filter.

Fig. 1.1 shows the structure of a FIR filter of order N. The input signal $x(t)$ is time-delayed using a delay line with N-1 taps, and each time-delayed component is multiplied by a coefficient, and then all the time-delayed components are added together. Mathematically, the output of the FIR filter in the time domain is given by

$$y(t) = \sum_{k=0}^{N-1} b_k x(t - kT) \tag{1.1}$$

where N is the number of taps, b_k is the coefficient of k-th tap, and T is the time delay difference between two adjacent taps. The free spectral range (FSR) of the filter is given by

$$FSR = \frac{1}{T} \tag{1.2}$$

By applying the Fourier Transform to both side of Equation (1.1), the transfer function of the filter can be obtained, which is given by

$$H(\omega) = \sum_{k=0}^{N-1} b_k e^{-j\omega kT} \tag{1.3}$$

As indicated in Equation (1.3), the filter response is determined by three parameters: the number of taps N, the coefficients $\{b_k\}$, and the time-delay

difference T. By properly choosing the values of these parameters, different filter functionalities, low-pass, band-pass or high-pass, can be implemented.

Based on the signal processing theory [1-3], if the coefficients of a filter are all positive, it can only function as a low-pass filter. In order to investigate the relationship between the filter response and the values of the coefficients $\{b_k\}$, we perform some simulations based on Equation (1.3). Fig. 1.2(a) shows the frequency response of a four-tap filter with all-positive coefficients $\{b_k\} = \{1,\ 1,\ 1,\ 1\}$. The time delay difference is 125 ps. As can be seen, it is a low-pass filter with a resonance peak at dc. For many applications, such as in electronic counter measures (ECM) and electronic support measures (ESM) systems, bandpass filters are highly desirable. In order to achieve bandpass filtering, some of the coefficients have to be negative. Fig. 1.2(b) shows the frequency response of a four-tap delay-line filter with both positive and negative coefficients $\{b_k\} = \{1, -1,\ 1, -1\}$. As can be seen, it is a bandpass filter with a notch at dc. Therefore, the generation of negative coefficients is essential to achieve bandpass filtering.

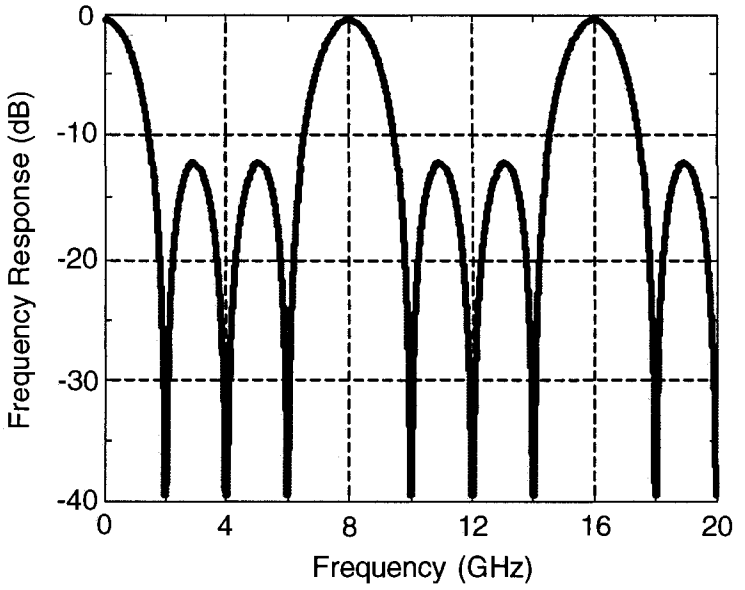

(a)

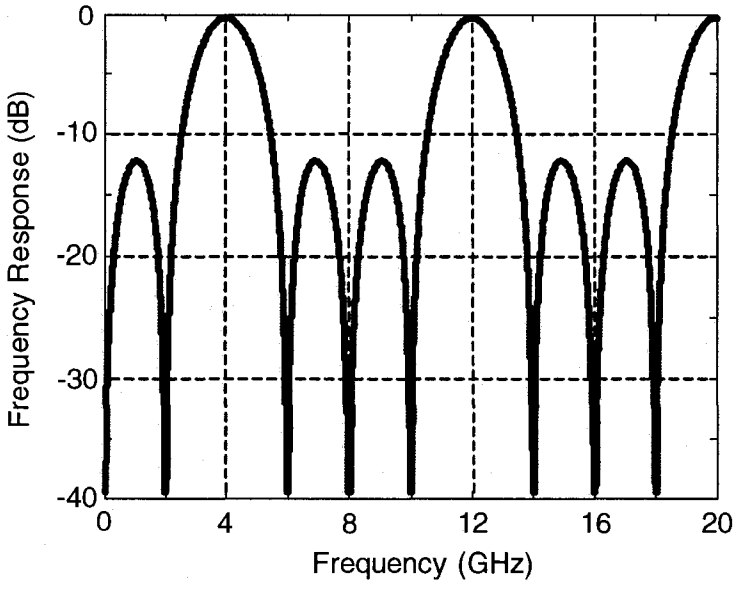

(b)

Fig. 1.2. Frequency response of a four-tap delay-line filter with a time delay difference of T = 125 ps, and coefficients of (a) $\{b_k\} = \{1,\ 1,\ 1,\ 1\}$, and (b) $\{b_k\} = \{1, -1,\ 1, -1\}$.

Another important issue in designing a photonic microwave filter is the tunability. For many applications, such as in scanning receivers and in microwave test equipments [4], microwave filers with large tunability are highly desirable. The tunability is usually achieved by adjusting the time delay difference. Fig. 1.3 shows the simulated frequency response of a four-tap filter with coefficients of $\{b_k\} = \{1, -1, 1, -1\}$, and the time delay difference is T = 62.5 ps. The FSR of the filter shown in Fig. 1.3 is 16 GHz, which is different from that in Fig. 1.2(b) with a time delay difference of T = 125 ps and an FSR of 8 GHz.

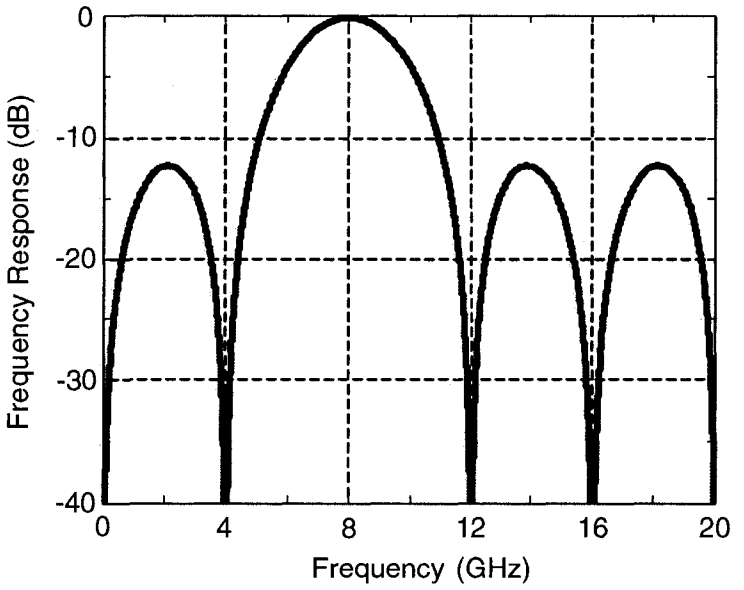

Fig. 1.3. Frequency response of a four-tap delay-line filter with a time delay difference of $T = 62.5$ ps, and coefficients of $\{b_k\} = \{1, -1, 1, -1\}$.

By comparing the filter responses in Fig. 1.2(b) and Fig. 1.3, we can see that by changing the time delay difference from 125 ps to 62.5 ps, the central frequency of the first mainlobe is shifted from 4 GHz to 8 GHz, and the frequency of the second notch is shifted from 2 GHz to 4 GHz. This characteristic enables us to tune the passband or stop-band frequency by changing the time delay.

However, it is also shown in Fig. 1.3 that the change of the time delay would lead to the change of the FSR, which results in the change of 3-dB bandwidth as well as the entire shape of the filter frequency response. For many applications, it is highly desirable that only the center frequency of the passband or stop-band be changed while keeping the shape of the frequency response unchanged. A solution to this problem is to use a microwave filter with complex coefficients. Fig. 1.4 shows the frequency response of a two-tap microwave filter with one positive and one complex coefficient. The frequency response can be expressed as

$$H(\omega) = 1 + e^{-j\theta} \cdot e^{-j\omega T} \tag{1.4}$$

where $e^{-j\theta}$ is the complex coefficient, and θ is the phase shift of the microwave signal, which is independent of the input microwave frequency. As can be seen in Fig. 1.4, by changing the microwave phase shift θ from 0 to 2π, the frequency response is also shifted, while keeping the entire shape and

the 3-dB bandwidth unchanged. This property is very important because we can design a tunable microwave filter while maintaining the shape of an optimized frequency response. The key to generating complex coefficients is to achieve a microwave phase shift that is independent of the input microwave frequency.

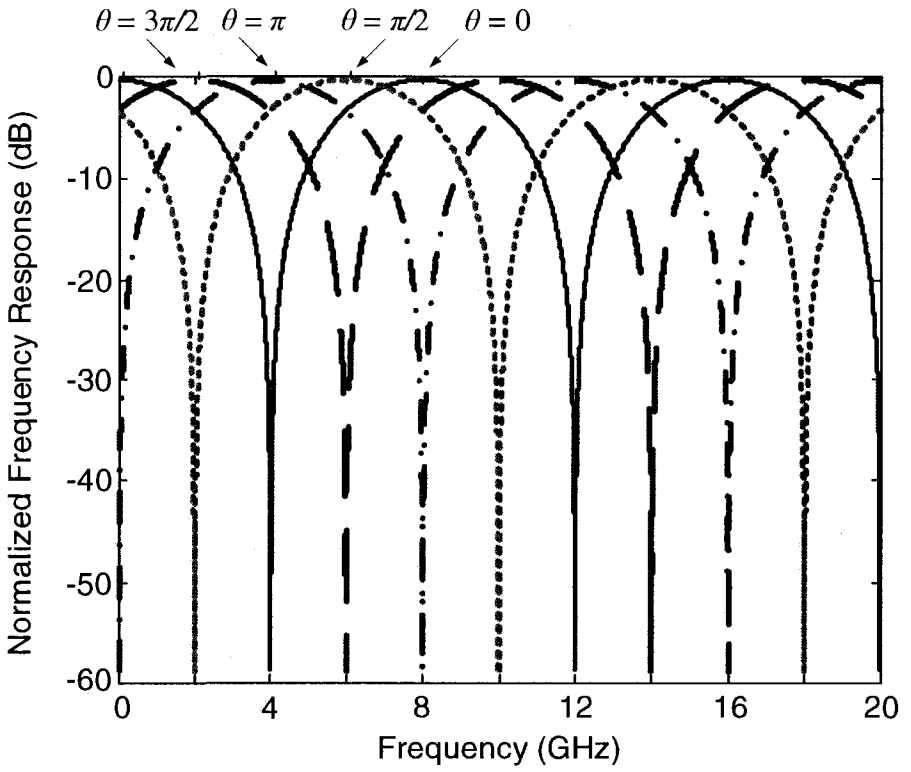

Fig. 1.4. Frequency response of a two-tap microwave filter with one complex coefficient: $H(\omega) = 1 + e^{-j\theta} \cdot e^{-j\omega T}$, where $\theta = 0, \frac{\pi}{2}, \pi, \frac{3\pi}{2}$.

1. 1. 2 Photonic microwave transversal filters

Photonic microwave filters are photonic systems designed to implement microwave filtering in the optical domain. Compared with the conventional electronic microwave filters, the photonic microwave filters have many advantages, such as high time bandwidth product, low loss, light weight, large tunability, high Q factor, and immunity to electromagnetic interference (EMI) [5-8]. In addition, since the microwave signals can be processed directly in the optical domain without the need of extra O/E and E/O conversions, the photonic microwave filters are of particular interest for applications such as optically controlled phased-array antennas and radio-over-fiber (RoF) systems.

Fig. 1.5 shows the general structure of a photonic microwave filter. Basically, a photonic microwave filter consists of an optical source, an electrooptic modulator, a time-delay device and a photodetector. The optical source can be a single narrowband laser source, an array of narrowband laser sources, or a broadband source such as ASE (Amplified Spontaneous Emission) or SLED (Superluminescent Light Emitting Diode) source. The continuous lightwave from the optical source is modulated by the RF input signal directly, or through an external electrooptic modulator, which can be an electrooptic intensity modulator (EOIM) or an electrooptic phase modulator (EOPM). The

modulated light is then fed into a time-delay device, to introduce different time delays with usually an identical time delay difference. The time delay device can be optical couplers, Mach-Zehnder lattices, a fiber Bragg grating (FBG) array, a chirped FBG, an Arrayed waveguide (AWG), a length of single mode fiber or high dispersion fiber, or other dispersive devices. The time-delayed signals are applied to the photodetector.

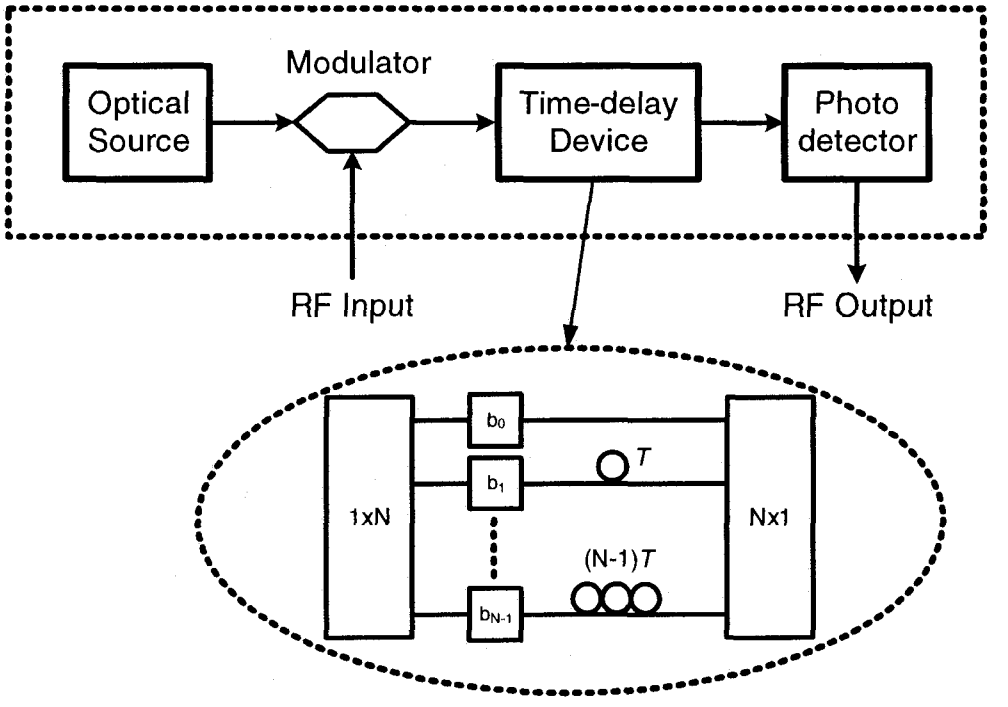

Fig. 1.5. General structure of a photonic microwave filter.

Based on the relationship between the coherence time τ_{coh} of the optical source and the unit time delay difference T of the filter, the photonic

microwave filters can be divided into two categories: "coherent" and "incoherent". The coherent time of an optical source is defined as

$$\tau_{coh} = \frac{1}{\pi \Delta v} \tag{1.5}$$

where Δv is the source linewidth in the absence of modulation. If $\tau_{coh} >> T$, the filter is said to be working under coherent regime, and it is possible to achieve negative coefficients using coherent detection [9-10]. However, under coherent regime, the filter transfer function is dependent on the optical phase shifts of the optical carrier, which are extremely sensitive to the environment. Therefore, coherent photonic microwave filters are difficult to be implemented under practical conditions. In order to avoid the optical interference and eliminate the influence of the environment, most reported photonic microwave filters are operating in the incoherent regime, where $\tau_{coh} << T$. In this case only optical intensities are added at the photodetector, and results in positive coefficients only.

The transfer function of the system shown in Fig. 1.5 can be expressed as

$$H(\omega) = \sum_{k=0}^{N-1} b_k e^{-j\omega kT} \tag{1.6}$$

which is the same as Equation (1.3). The FSR of the filter is determined by the unit time delay difference T, and the tap weight b_k is proportional to the

optical intensity of the k-th optical path and cannot be negative. Based on the analysis in Section 1.1.1, a filter with all-positive coefficients can only function as a low-pass filter. This results in a severe limitation on the functionalities of the photonic microwave filters, such as bandpass and highpass, etc. In order to overcome this limitation, various approaches have been proposed to generate negative and complex coefficients under incoherent regime. In the next section, a review of recent approaches proposed to implement photonic microwave filters with negative and complex coefficients is presented.

1.2 Background review

In 1976, Wilner and Van den Heuvel were the first to propose [11] that optical fibers are promising to be utilized for delay line signal processing, because the optical fibers have very low loss, and can provide very high time-bandwidth products for delay lines. Since the 1980's, extensive work has been done to implement photonic microwave filters with different configurations. In terms of the structure of the time-delay device, the proposed approaches can be divided into the following categories, which are based on optical couplers [12-14], FBGs [15-23], AWG [24-25], Mach-Zehnder lattices [26], or a length of dispersive fiber [27-28]. To avoid optical interference, most of the proposed

approaches are operated in the incoherent regime, leading to all-positive coefficients and hence low-pass filtering only. In order to overcome this limitation, considerable efforts have been taken to achieve negative coefficients and consequently realize bandpass filtering in the incoherent regime.

1.2.1 Photonic microwave filters with negative coefficients

One approach to achieve negative coefficients is using differential detection [13] [29]. As shown in Fig. 1.6, the lightwave from the optical source is modulated by the input RF signal, and time delayed through optical fiber delay lines. The output signals from the fiber delay lines are fed to a differential photodetector. The output of the two matched photodetectors are combined and subtracted electrically, leading to the generation of a positive and a negative coefficient corresponding to the upper or the lower photodetector, respectively. In this approach, the negative coefficient was not achieved directly in the optical domain, instead it was achieved in the electrical domain based on differential photodetection, which increases the complexity of the system.

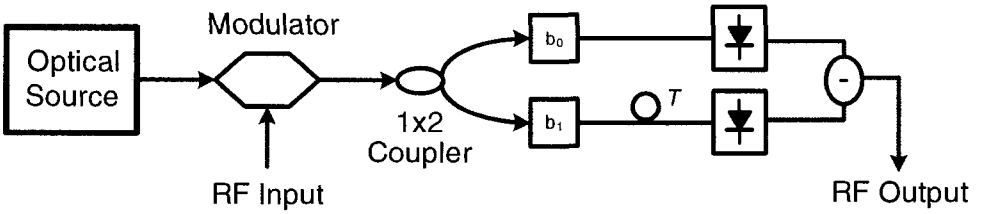

Fig. 1.6. Photonic microwave filter with negative coefficients using differential detection

To generate negative coefficients directly in the optical domain without extra O/E and E/O conversions, several techniques have been proposed. One approach is using wavelength conversion based on cross-gain saturation modulation in a semiconductor optical amplifier (SOA) [30]. As shown in Fig. 1.7, a tunable laser source operating at λ_1 is modulated by the input RF signal, and then split into two parts. One part goes through a length of optical fiber, which introduces a time delay. The other part is combined with the output continuous wave (CW) beam from a distributed feedback (DFB) laser operating at a different wavelength λ_2, and then fed into an SOA. Due to cross-gain modulation in the SOA [31], the CW beam λ_2 is also modulated by the input RF signal, but with a π phase inversion compared with the RF signal carried by λ_1, leading to the generation of a negative coefficient. Using an optical bandpass filter, λ_1 is filtered out and only λ_2 can go through. Then, the time-delayed RF signal carried by λ_1 in the upper route and the π-phase-

inverted RF signal carried by λ_2 in the lower route is combined and detected by the photodetector. Thus, a two-tap photonic microwave bandpass filter with one negative coefficient is implemented.

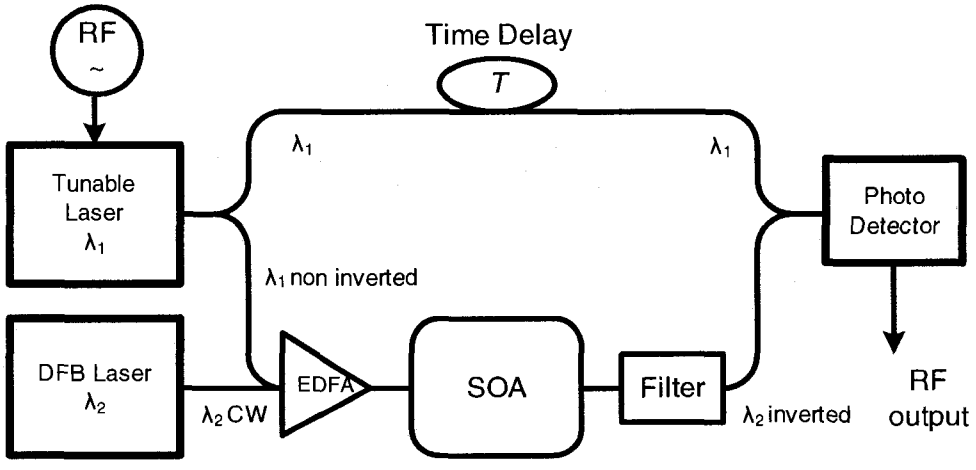

Fig. 1.7. Photonic microwave filter with a negative coefficient based on cross gain modulation in an SOA.

Another technique to generate a negative coefficient is based on injection-locked Fabry-Perot (FP) laser diode and fiber Bragg gratings (FBGs) [32]. As shown in Fig. 1.8, the output of a tunable laser source is modulated by the input RF signal through an electrooptic intensity modulator, and divided into two parts. One part goes through a length of fiber, and the other part is injected into an FP laser diode. The FP laser is biased above its threshold. Due to the cross-intensity modulation among the longitudinal modes of the FP laser

diode, the intensity of the injection-locked longitudinal mode is modulated by the injected modulating RF signal, while the intensity of the unlocked longitudinal mode is inversely modulated by the modulating signal. As a result, the injection-locked modes can act as positive taps, and the unlocked modes can act as negative taps. Then, the output optical signal from the FP laser diode is fed into a tunable FBG array, and different modes are reflected by different FBGs, to introduce time delay difference between the taps. As shown in Fig. 1.8, for the upper part of the configuration, the modulated optical signal from the tunable laser source can provide an additional positive tap by properly adjusting the fiber length.

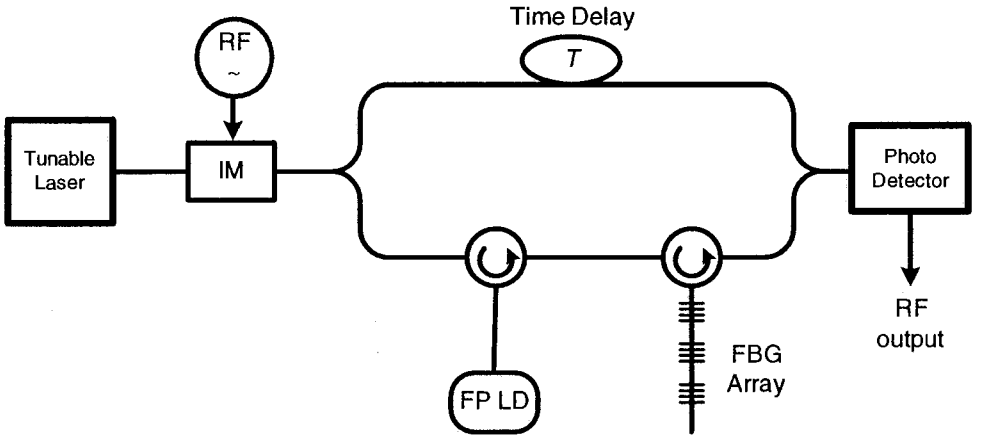

Fig. 1.8. Photonic microwave filter with negative coefficients based on an injection-locked FP laser diode and FBGs.

Negative coefficients can also be generated by using the carrier depletion effect in a DFB laser diode [33].

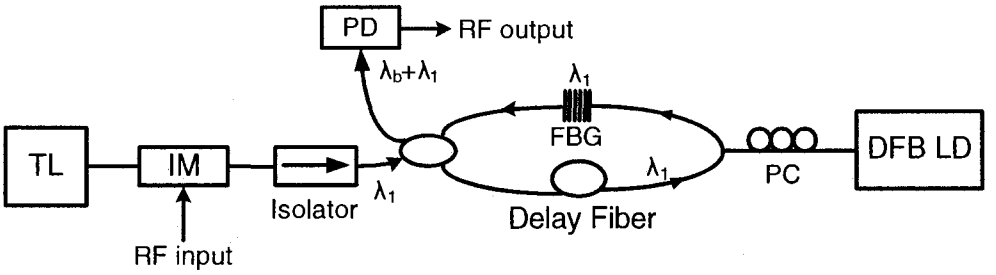

Fig. 1.9. Photonic microwave filter with negative coefficients based on carrier depletion effect in a DFB laser diode.

As shown in Fig. 1.9, the output optical signal from a tunable laser source operating at wavelength λ_1 is split into two parts. One part goes directly to the FBG with central reflection wavelength of λ_1 and is reflected back. The other part goes through a length of optical fiber and then injects into the DFB laser diode, which is biased above threshold. Due to the carrier depletion effect in the DFB laser diode [34], the modulation is transferred from the incoming wavelength λ_1 to the Bragg wavelength λ_b of the DFB laser diode with a reversed polarity. As a result, the RF modulating signal is carried by λ_b with a π phase inversion, which can be directly utilized to generate a negative coefficient in a photonic microwave filter. The optical signal at wavelength λ_b

can pass through the FBG, and the residual light at λ_1 is filtered out by the FBG. By using an FBG array or a chirped FBG, discrete or continuous tuning of the filter response can be achieved through tuning the wavelength of the tunable laser source.

More recently, a new technique based on two electro-optic intensity modulators (EOIM) biased at opposite transmission slopes was reported for the implementation of photonic microwave bandpass filter with negative coefficients [35]. The principle of the RF phase inversion in the proposed approach is shown in Fig. 1.10. As can be seen, there are two linear modulation regions in the sinusoidal transfer function of an EOIM, centered at V_{BIAS}^{-} and V_{BIAS}^{+}. When the EOIM is biased at V_{BIAS}^{+}, the input RF signal is applied to the positive slope of the transfer function. If the output of the EOIM is detected by a photodetector, the recovered RF signal will be in-phase with the input RF modulating signal. On the contrary, if the EOIM is biased at V_{BIAS}^{-}, the negative slope of the transfer function is utilized. Consequently, the recovered RF signal will be π out-of-phase with the input RF modulating signal.

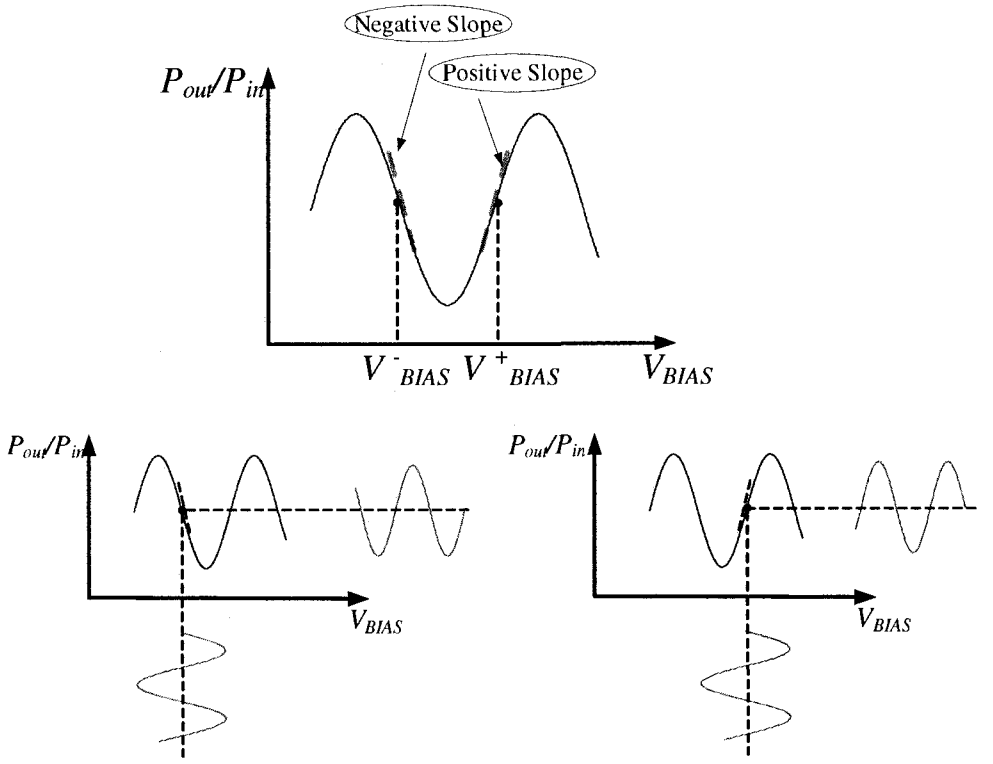

Fig. 1.10. Phase inversion of the RF modulating signal by changing the bias point of the EOIM.

This characteristic can be employed to implement photonic microwave bandpass filter with negative coefficients, as shown in Fig. 1.11. The output optical signals from two tunable laser sources operating at different wavelengths are modulated by the same input RF signal through two EOIMs. The EOIMs are biased at V^-_{BIAS} (negative tap) and V^+_{BIAS} (positive tap). The output modulated optical signals from the EOIMs are combined and fed into a dispersive device, which can be a length of optical fiber or a chirped FBG, to

introduce a time delay difference between the two taps. Compared with other techniques, the advantage of the proposed approach is that it is easy to extend to a multi-tap photonic microwave filter with positive and negative coefficients by simply adding more tunable laser sources to the upper or lower part of the filter, corresponding to the positive or negative taps.

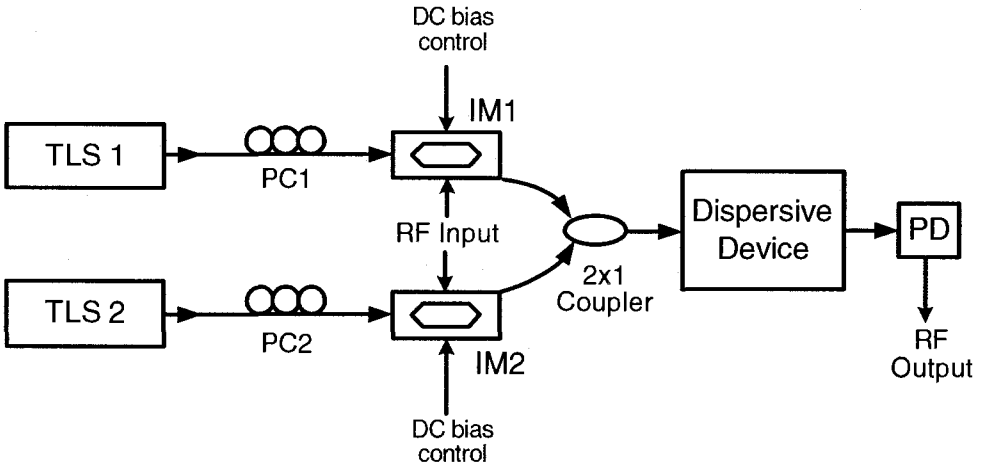

Fig. 1.11. Photonic microwave filter with negative coefficients based on two EOIMs at different bias points.

Another approach for implementing a photonic microwave filter with negative coefficients was proposed recently [36]. As shown in Fig. 1.12, the output signal from a broadband ASE source (EDFA) is transmitted through a uniform FBG. The transmission spectrum of the EDFA is carved by the transmission spectrum of the FBG, which can act as the negative tap of the filter, as shown

in Fig. 1.12. The positive tap is provided by the output of a tunable laser source. The two optical signals are then combined and modulated by the input RF signal. The drawback of this technique is that there is always a DC component presenting in the frequency response. This is because the average optical level is nonzero. This limitation can be overcome by using a DC blocker in electrical domain.

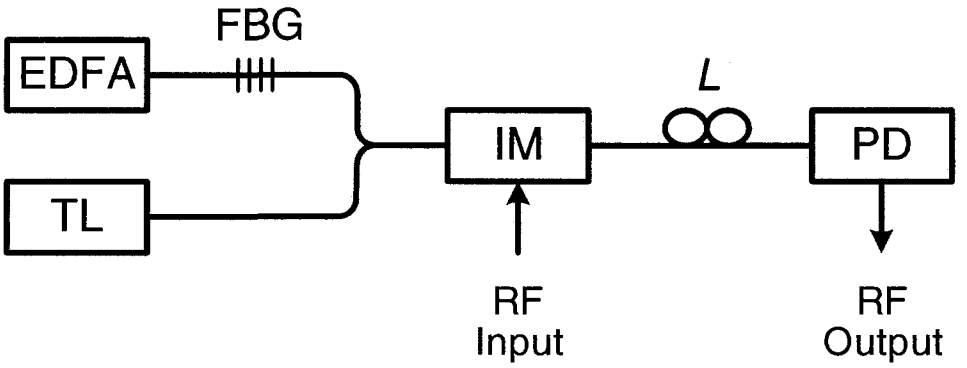

Fig. 1.12. Photonic microwave filter with negative coefficients based on broadband ASE spectrum transmitted through an FBG.

Recently, a novel method to realize a photonic microwave bandpass filter with negative coefficients using a phase modulator was proposed [37]. By reflecting the phase modulated optical signals from linearly chirped FBGs (LCFBGs) with positive or negative dispersions, phase modulation is converted to intensity modulation, with recovered microwave signals having positive and negative polarities.

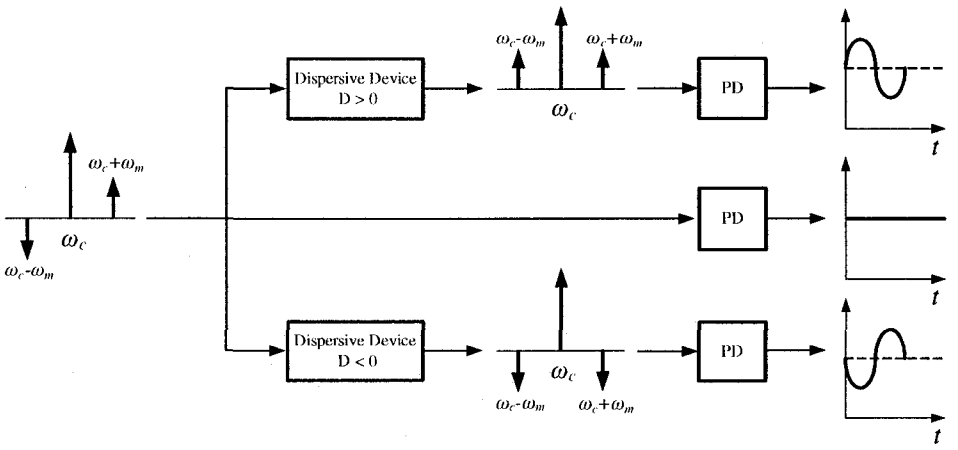

Fig. 1.13. RF phase inversion based on PM-IM conversion through opposite dispersions.

The fundamental concept is shown in Fig. 1.13. If the phase modulated signal is directly detected using a PD, the modulating signal cannot be recovered and only a dc signal can be obtained because the beating between the carrier and the upper sideband exactly cancels the beating between the carrier and the lower sideband. However, if the modulated optical signal passes through a dispersive device, the phase modulation can be converted to intensity modulation. Moreover, for different signs of the dispersions, the recovered RF signals will have a π phase inversion, which can be applied to implement negative coefficients in a photonic microwave filter. The system configuration of the filter is shown in Fig. 1.14.

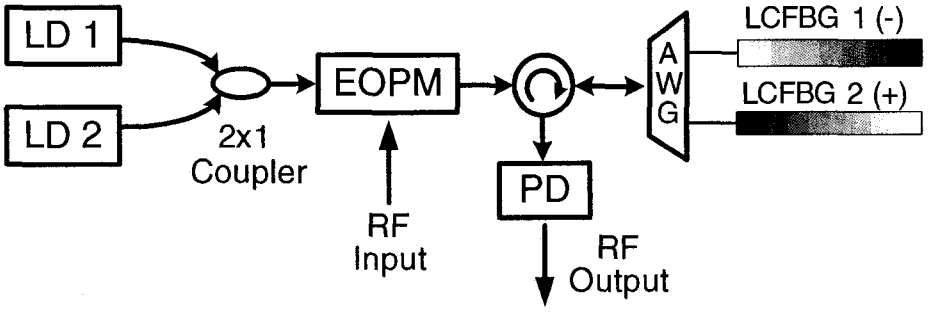

Fig. 1.14. System configuration of a photonic microwave filter with a negative coefficient based on PM-IM conversion in two LCFBGs with opposite dispersions.

Another novel and simple technique to implement photonic microwave filter with negative coefficients based on PM-IM conversion was proposed in [38]. The negative coefficients are generated through PM-IM conversion by an optical filter serving as a frequency discriminator. As shown in Fig. 1.15, the optical carriers from two laser sources are phase modulated by the input RF signal, and then fed into an optical filter. The carriers are tuned at the opposite slopes of the optical transfer function of the optical filter. As a result, the phase-modulated signals are converted to intensity-modulated signals, with π out of phase depending on the carrier position at positive or negative slope of the optical filter.

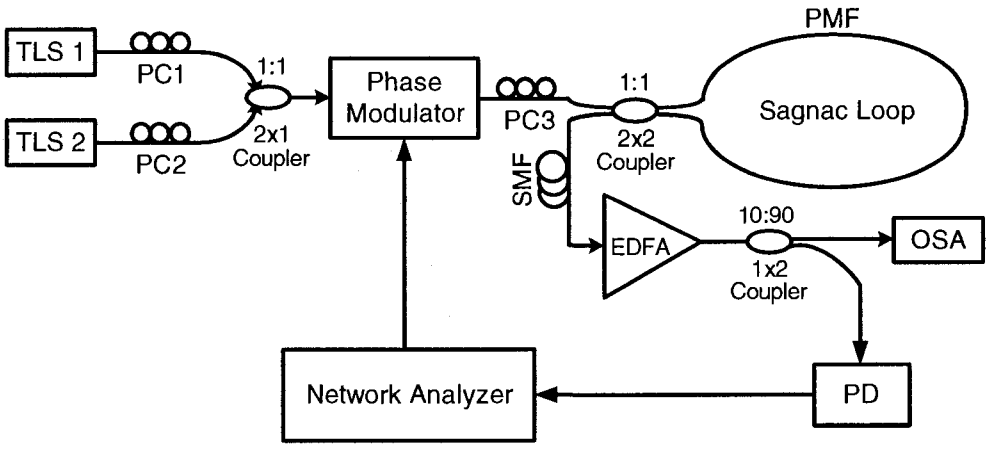

Fig. 1.15. Photonic microwave filter with negative coefficients based on PM-IM conversion using an optical filter.

Recently, a new and simple photonic microwave bandpass filter with negative coefficients based on polarization modulation in an electro-optic polarization modulator (PolM) was proposed and demonstrated [39]. As shown in Fig. 1.16 [39], the output lightwave from a tunable laser source is sent to a PolM, which is modulated by the input RF signal. Due to the polarization modulation at the PolM, two out-of-phase RF signals carried by two optical carriers with orthogonal polarizations are achieved at the output of the PolM. Then, the optical microwave signals are fed into a section or two sections of polarization maintaining fiber (PMF) to generate time delays. A photonic microwave bandpass filter of two or four taps with negative coefficients was experimentally demonstrated, as shown in Fig. 1.16.

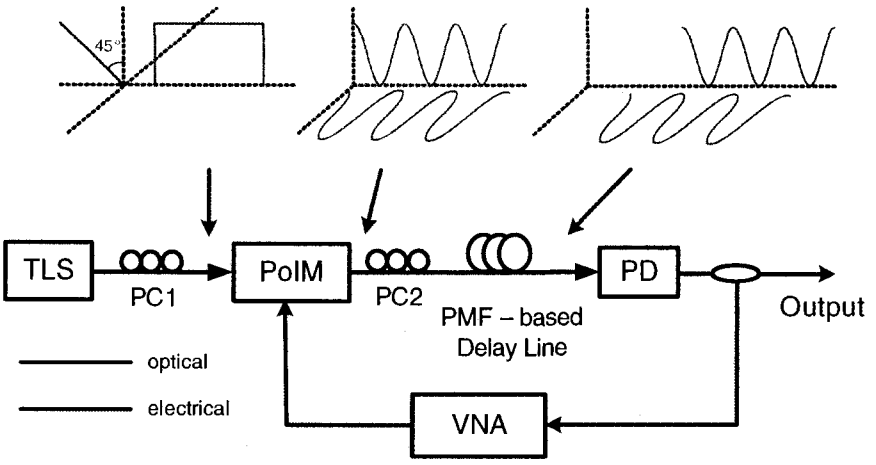

Fig. 1.16. Photonic microwave filter with negative coefficients based on polarization modulator (PolM).

1.2.2 Photonic microwave filters with complex coefficients

As discussed in Section 1.1.2, the tunability of the filter is usually achieved by adjusting the time delay difference. However, the change of the time delay difference would lead to changes in the FSR, which results in the change of 3-dB bandwidth as well as the entire shape of the filter frequency response. For many applications, it is highly desirable that only the center frequency of the passband or stop-band be changed while keeping the shape of the frequency response unchanged. A solution to this problem is to use a photonic microwave filter with complex coefficients.

Two configurations have been recently reported [40] [41] for the implementation of tunable microwave filters with complex coefficients. In [40], the complex coefficient was generated in a system using three optical attenuators and two microwave couplers.

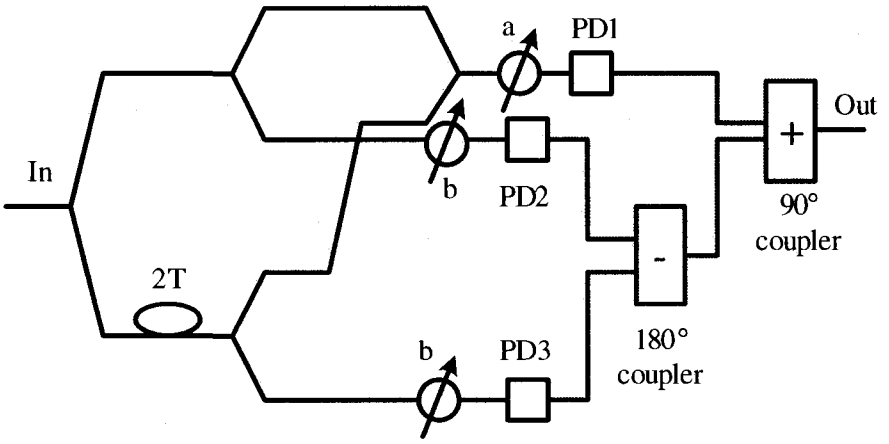

Fig. 1.17. Photonic microwave filter with complex coefficients using three optical attenuators and two microwave couplers.

As shown in Fig. 1.17, the transfer function of the system can be written as

$$H(f)=\frac{a}{2}(e^{j2\pi fT}+e^{-j2\pi fT})-\frac{b}{2j}(e^{j2\pi fT}-e^{-j2\pi fT}) \tag{1.7}$$

If we let $a=\cos(\varphi), b=\sin(\varphi)$, the transfer function can be written as

$$H(f)=\cos(2\pi fT+\varphi) \tag{1.8}$$

Therefore, by changing the values of a and b, the notch frequency of the filter can be tuned, and the FSR and 3-dB bandwidth are maintained independent of tuning. The frequency response of the filter when the notch frequency is tuned is shown in Fig. 1.18. Since the values of a and b is changed by using optical attenuators, the tuning range of a and b is from 0 to 1, which limits the RF phase shift from 0 to 180° or a tunable range of a half FSR, as shown in Fig. 1.18. Moreover, the complex coefficient is generated in the electrical domain.

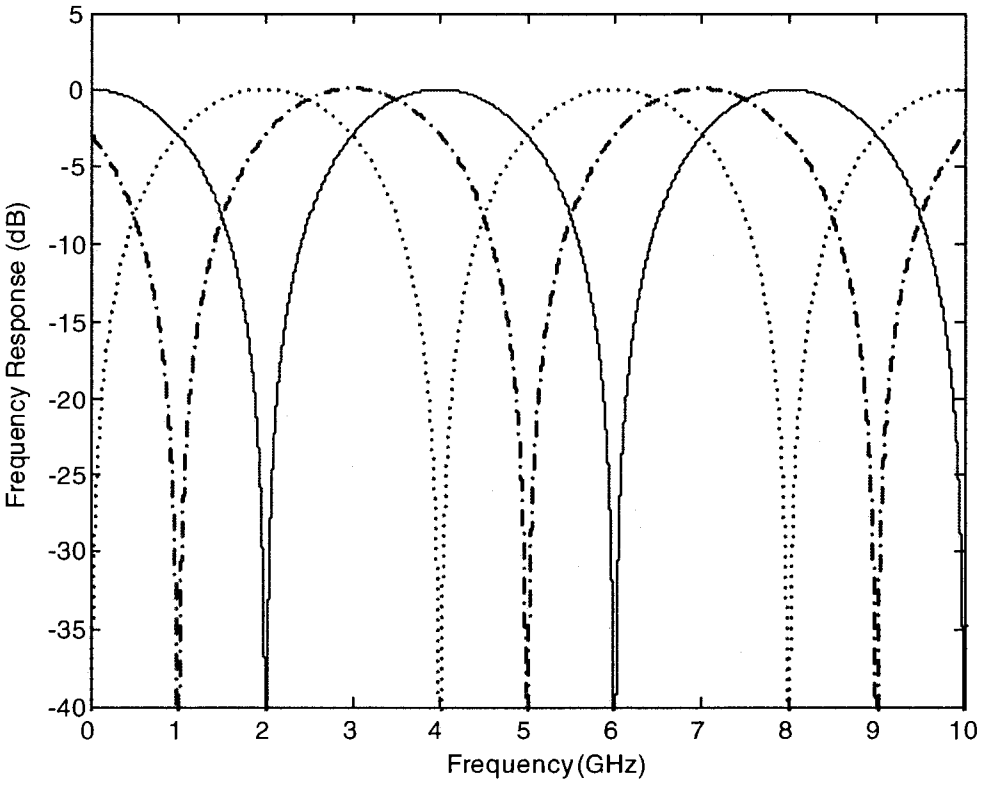

Fig. 1.18, Frequency response of photonic microwave filter with complex coefficients. Solid: $a = 1$, $b = 0$; dotted: $a = 0$, $b = 1$; dash-dot: $a = b = 0.71$.

To achieve complex coefficients directly in the optical domain, a tunable photonic microwave filter based on a tunable optically induced RF phase shift was proposed [41]. In the system, the complex coefficient was generated by changing the phase of the RF signal, which was realized based on a combined use of optical single-sideband modulation (SSB) and stimulated Brillouin scattering (SBS). The experimental setup is shown in Fig. 1.19 [41].

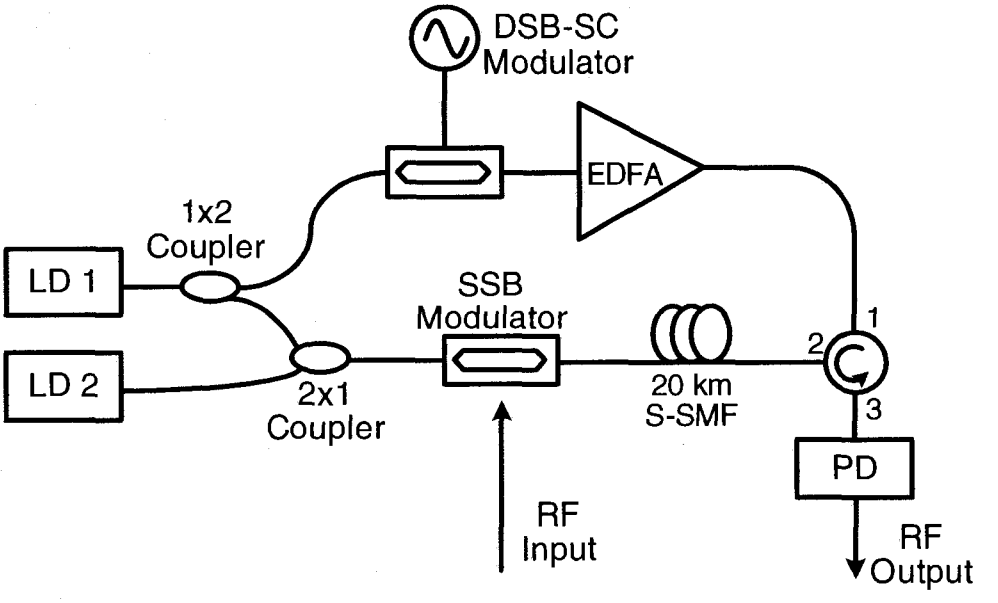

Fig. 1.19. Photonic microwave filter with complex coefficients based on SSB and SBS.

In [41], to stimulate the SBS, a 20-km single mode fiber was used, which makes the system bulky. To avoid using a long optical fiber, we propose a

novel tunable photonic microwave filter with complex coefficients with a very simple structure, which will be discussed in Chapter 4.

1.3 Major contributions of this research

1. A photonic microwave bandpass filter with negative coefficients based on cross-polarization-modulation (XPolM) in a semiconductor optical amplifier (SOA) is proposed and experimentally implemented. The impact of the SOA cross gain modulation (XGM) on the performance of the microwave filter is also investigated.

2. A continuously tunable photonic microwave bandpass filter with positive and negative coefficients using an optical phase modulator and chirped FBGs is proposed and experimentally demonstrated. The positive and negative coefficients are generated through PM-IM conversion by reflecting the phase-modulated optical carrier from LCFBGs with positive and negative dispersions. The tunability of the filter is realized by changing the wavelength of the optical carrier such that it is reflected at different physical locations in the LCFBGs. A two-tap microwave bandpass filter with an FSR tunable from 1.14 to 4.55 GHz is experimentally demonstrated.

3. A novel tunable microwave filter with complex coefficients using a wideband tunable optical RF phase shifter that consists of two electro-optic intensity modulators is proposed and experimentally demonstrated. By simply adjusting the bias voltages applied to the two intensity modulators, the filter response can be continuously tuned, and the 3-dB bandwidth and the shape of the filter response can be maintained unchanged. A two-tap photonic microwave filter with one tunable complex coefficient, with a wide and continuous tuning range, is experimentally demonstrated.

4. A technique to improve the dynamic range of a photonic microwave bandpass filter is proposed and experimentally investigated. The bandpass filter is implemented based on PM-IM conversion using FBGs serving as frequency discriminators. The dynamic range of the filter is increased by reducing the optical-carrier-induced shot noise and relative intensity noise (RIN) at the photodetector, which is realized by placing the optical carriers at the locations closer to the bottoms of the FBG reflection spectra. An improvement of dynamic range of about 10 dB is realized with this technique.

Chapter 2

PHOTONIC MICROWAVE BANDPASS FILTER BASED ON CROSS POLARIZATION MODULATION IN A SEMICONDUCTOR OPTICAL AMPLIFIER

In order to avoid optical interference in optical microwave filters, a low-coherence light source is usually used. For many applications, such as in an RoF system, the optical sources are telecom-type laser diodes with high coherence. In [42], an approach was proposed to implement an optical fiber delay line filter that is free of limitation imposed by optical coherence. In the proposed filter, the time delay difference was introduced by passing the modulated optical signal through a high birefringence (Hi-Bi) fiber, with the two polarization modes traveling at different velocities along the fast and the slow axes. Due to the orthogonality of the two polarization states, no optical interference would be generated. However, the approach proposed in [42] can only realize a microwave filter with all-positive coefficients. Recently, an approach implementing an optical microwave filter with negative coefficients based on cross polarization modulation (XPolM) in a highly nonlinear fiber

(HNLF) was proposed [43]. In the system, an optical pump that was intensity-modulated by a microwave signal was injected with a continuous wave (CW) probe into the HNLF, in which the two orthogonal polarization modes of the probe were polarization modulated by the pump, with two microwave signals that were out of phase on the two polarization modes. After traveling in a Hi-Bi fiber, the two polarization modes would experience different time delays. At the output of a PD, the two out-of-phase microwave signals were obtained. Therefore, a two-tap optical microwave filter with a negative coefficient was realized. The use of a HNLF to implement XPolM has some limitations. First, to introduce enough XPolM the HNLF should have a long length, which makes the system bulky. Second, the polarization states in the long HNLF would suffer from the environmental changes, which would affect the system stability. Third, the effect of stimulated Brillouin scattering (SBS) in the HNLF impose a limit on the input pump power level, thus limiting the XPolM efficiency.

XPolM can also be generated in a semiconductor optical amplifier (SOA) [44] [45]. Compared with the HNLF-based XPolM, the SOA-based XPolM has the advantages of simple configuration, small package, and ease of integration. Another key advantage of the SOA-based XPolM is that the system will not

suffer from the effect of SBS, which is easy to take place in a HNLF. The SBS power threshold of the HNLF is [51]

$$P_{SBS} \approx \frac{21A_{eff}}{g_0 L_{eff}} \tag{2.3}$$

where P_{SBS} is the SBS threshold, A_{eff} is the effective area of the light mode, g_0 is the peak value of the Lorentzian-shaped Brillouin gain spectrum, and L_{eff} is the effective interaction length. The typical parameters of the HNLF are [52]: $A_{eff} = 12$ μm^2, $g_0 = 5.8 \times 10^{-11}$ m/W. The calculated SBS power threshold for 1.5-km HNLF is 4.6 dBm, which imposes an upper limit on the input power level and limits the XPolM efficiency. Since the SBS effect does not exist in an SOA, the input powers can be higher, to increase the XPolM efficiency.

In this chapter, we demonstrate an all-optical microwave bandpass filter with negative coefficients based on XPolM in an SOA, as shown in Fig. 2.1. In the proposed configuration, the polarization of a continuous wave (CW) probe from a laser diode (LD) is modulated in the SOA by a pump light that is intensity modulated by a microwave signal. The cross-polarization modulated probe at the output of the SOA has two orthogonal polarization modes. One mode carries the inverted signal compared to the input pump signal, and the other carries the non-inverted signal. Since the two microwave signals carried

by the two polarization modes are out of phase, the inverted and the non-inverted signals act as the positive and the negative coefficients of the filter. In order to introduce a time delay difference, the probe is then fed to a length of Hi-Bi fiber. The use of an SOA will introduce XGM, which is much stronger than XPolM and makes the inverted signal much stronger than the non-inverted signal, leading to a significant filter coefficient difference. For a microwave filter with many taps, some of the coefficients may be much smaller than the others, in order to have an optimized transfer function [46]. For a microwave filter with a few taps, we may want the delay signals to have similar contributions to the filter response. Therefore, the suppression of the XGM in the proposed filter is an issue that needs to be examined. We find that by increasing the pump power, both the XGM and the XPolM become stronger, but the efficiency of the XPolM increases faster than that of the XGM. On the other hand, by increasing the probe power, the XGM can be reduced. By optimizing the powers of the pump and the probe, the coefficient difference can be minimized. However, in our experiment, the inverted signal still has an amplitude that is about 4 times higher than that of the non-inverted signal. To further reduce the coefficient difference, we propose to incorporate a tunable polarizer after the Hi-Bi fiber in the system. The transmission axis of the tunable polarizer is adjusted such that the non-inverted signal has a higher projection on the transmission axis of the polarizer compared to the inverted

signal. By tuning the angle of the transmission axis of the tunable polarizer, the filter coefficients can also be tuned, therefore a photonic microwave filter that is reconfigurable is implemented. The time-delayed signals after the tunable polarizer are detected at a photodetector (PD). Since the microwave signals carried by the two polarization modes are out of phase, a microwave filter with one negative and one positive coefficient is achieved.

2.1 Principles

The schematic diagram of the proposed filter is shown in Fig. 2.1. A tunable laser source is used to generate a CW probe at λ_1. The microwave signal to be processed is carried by a pump at a different wavelength λ_2. The polarization directions between the two beams are adjusted to be 45°. Originally, the polarization state of the probe beam is along the y-axis, as shown in Fig. 2.1. With the injection of the pump, additional birefringence is generated in the SOA [44], which causes the transverse electric (TE) and transverse magnetic (TM) modes of the probe to experience a different refractive index given by [45], [47]

$$N_{TE}(n) = N_{TE0} + \Gamma_{TE} n\left(\frac{dN_{TE}}{dn}\right) \tag{2.1a}$$

$$N_{TM}(n) = N_{TM0} + \Gamma_{TM} n\left(\frac{dN_{TM}}{dn}\right) \tag{2.1b}$$

where n is the carrier density, N_0 is the refractive index of the waveguide for zero carrier density, Γ is the confinement factor, and (dN/dn) is the differential refractive index. The phase shift of the TM or TE modes of the probe due to the injection of the pump light is given by

$$\varphi_{\mathrm{TM/TE}} = \frac{2\pi L}{\lambda_1}\left(N_{\mathrm{TM/TE}} + \Gamma_{\mathrm{TM/TE}} n_p \frac{dN_{\mathrm{TM/TE}}}{dn}\right) + \frac{2\pi L \Gamma_{\mathrm{TM/TE}}(n - n_0)}{\lambda_1}\frac{dN_{\mathrm{TM/TE}}}{dn} \tag{2.2}$$

where $\varphi_{TM/TE}$ is the phase shift of the TM or TE mode, L is the length of the SOA, λ_1 is the wavelength of the probe light, n_p is the value of the carrier concentration for zero input power at the bias current used to define the peak gain wavelength, and n_0 is the transparency carrier concentration. The phase shift is different for the TE and TM modes of the probe because of the TE/TM asymmetry in both the confinement factors and effective guide refractive indices of the SOA [45].

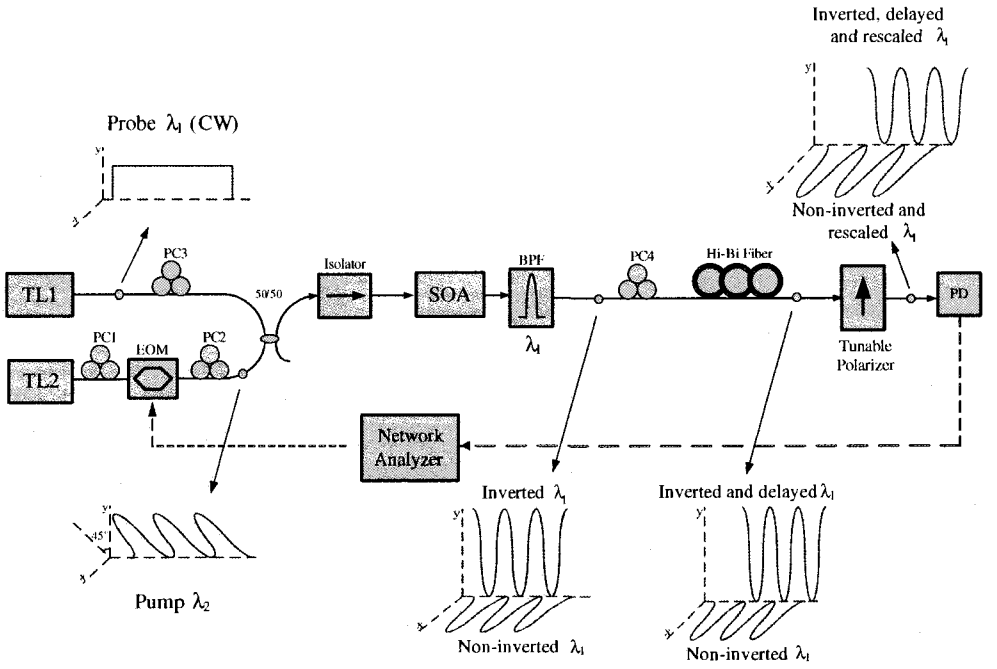

Fig. 2.1. Schematic diagram of the optical microwave bandpass filter with a negative coefficient based on XPolM in SOA. BPF: bandpass filter.

As a consequence, the polarization of the probe beam is rotated [48]-[50], part of the probe is projected to the x-axis. An increase in the intensity of the pump leads to an increase in the intensity of the probe along the x-axis, which carries the non-inverted signal of the pump. On the contrary, an increase in the intensity of the pump leads to a decrease in the intensity of the probe along the y-axis, which carries the inverted signal of the pump. Consequently, the non-inverted signal appears along the x-axis, and the inverted signal appears along the y-axis. A photodetection of the signals would generate two microwave signals that are out of phase.

As can be seen in Fig. 2.1, a bandpass filter (BPF) with a center wavelength at λ_1 is incorporated to eliminate the pump signal after the XPolM. The two polarization modes of the probe are then sent to a delay line to generate a time delay difference. This is realized in the proposed system by using a Hi-Bi fiber. Due to the birefringence of the Hi-Bi fiber, the two polarization modes would travel along the fast and slow axes with different velocities, leading to a time delay difference. In the filter design, the time delay difference can be controlled by changing the length of the Hi-Bi fiber, which enables the filter to have a required free spectral range (FSR).

In addition to the XPolM in the SOA, the injection of a high-power pump together with a probe would lead to the generation of XGM, which transfers the signal carried by the pump to the probe with a reversed polarity. As a result, the inverted signal is enhanced, while the non-inverted signal is reduced, a significant difference of the filter coefficients is observed.

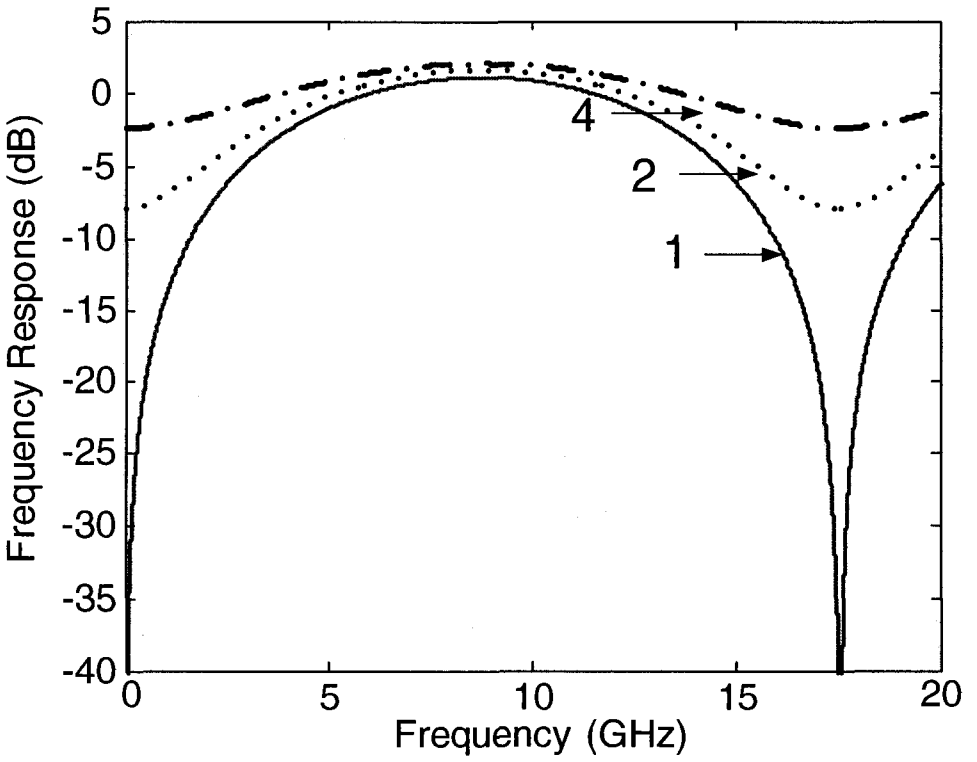

Fig. 2.2. Numerical simulation of the frequency response corresponding to different ratios of the positive and negative coefficients (solid: ratio = 1, dotted: ratio = 2, and dash-dot: ratio = 4).

A numerical simulation of the frequency response corresponding to different ratios of the positive and negative coefficients is shown in Fig. 2.2. It can be seen that the filter is reconfigurable if the coefficient ratio is tunable. To have large reconfigurability, we expect that the ratio has a large tunable range, for example, from a large value down to 1.

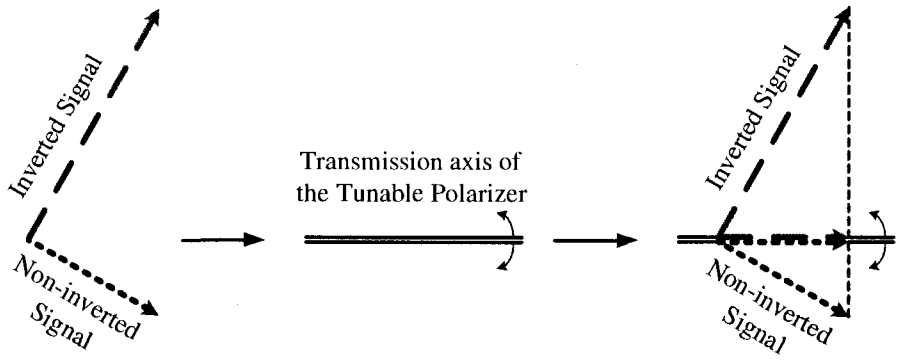

Fig. 2.3. Tuning the ratio between the inverted and non-inverted signals using a tunable polarizer.

To make the ratio have a large adjustable range, we have to minimize the ratio between the powers of the inverted and non-inverted microwave signals. The ratio can be reduced if we increase the input powers of the pump and the probe. We find that both the XGM and the XPolM become stronger when the pump power is increased, but the efficiency of the XPolM is increased faster than that of the XGM. As a result, the impact of the XGM can be reduced. In the next section, we will show that when the input pump and the probe powers are increased, the ratio can be reduced to close to 4. To further reduce the ratio, we propose to use a tunable polarizer after the Hi-Bi fiber. As can be seen from Fig. 2.3, after traveling along the two axes of the Hi-Bi fiber, the time-delayed signals will be projected onto the transmission axis of the polarizer. The tunable polarizer is adjusted in such a way that the transmission axis is

closer to the non-inverted signal, which is weaker than the inverted signal. Consequently, the projection of the non-inverted signal onto the transmission axis can be equal to the projection of the inverted signal, and thus the ratio of the two coefficients can be adjusted to 1. By tuning the transmission axis of the tunable polarizer, the ratio of the coefficients can be controlled. Therefore, a reconfigurable filter with tunable coefficients can be easily implemented.

2.2 Experiments and discussions

Experiments based on the configuration shown in Fig. 2.1 are performed. A CW tunable laser source (TL1) with a typical linewidth of 150 kHz is employed to generate the probe. The wavelength of the probe is set at 1548.85 nm. A second tunable laser source (TL2) is used to generate the pump. The wavelength of the pump is set at 1552.82 nm, which is modulated by a microwave signal from a Vector Network Analyzer (VNA) using a LiNbO3 electro-optic intensity modulator (EOM). A polarization controller (PC1) is connected between TLS2 and the EOM to align the polarization direction of the pump light with the principal axis of the EOM. The powers of the pump and the probe are -2 and -3.3 dBm, respectively. Two other polarization controllers, PC2 and PC3, are used to adjust the polarization directions of the pump and probe. The polarization direction of the probe is adjusted to align

with the y-axis, and that of the pump is adjusted to be at 45° with respect to the probe. The SOA (JDS-U, CQF 872) used in the experiment has a peak small signal gain of 26.9 dB (at 1532 nm) and a 3-dB saturation power of 10.1 dBm at 300-mA driving current. In the experiment, the bias current of the SOA is set at 300 mA. To eliminate the pump signal after the XPolM, a BPF with a 3-dB bandwidth of 0.2 nm is connected after the SOA. The inclusion of the BPF also helps suppress the amplified spontaneous emission (ASE) noise of the SOA. A fourth polarization controller, PC4, is used to align the two polarization modes of the probe with the slow and fast axes of the Hi-Bi fiber. In the experiment, 42-m Hi-Bi fiber (Corning PM1550, beating length = 3.75 mm) is used, which provides a time delay difference of 57 ps. The tunable polarizer adjusts the powers of two time-delayed signals, which are then detected by the PD.

We first investigate the generation of the two out-of-phase signals based on XPolM. A 10-GHz sinusoidal signal is applied to the EOM to modulate the pump carrier. A tunable linear polarizer is connected after the BPF. By adjusting the transmission axis of the tunable polarizer to align it with the polarization direction of one of the two polarization modes, we can select one of the two modes. The recovered microwave signal at the PD is then observed on an oscilloscope (Agilent 86100C), as shown in Fig. 2.4.

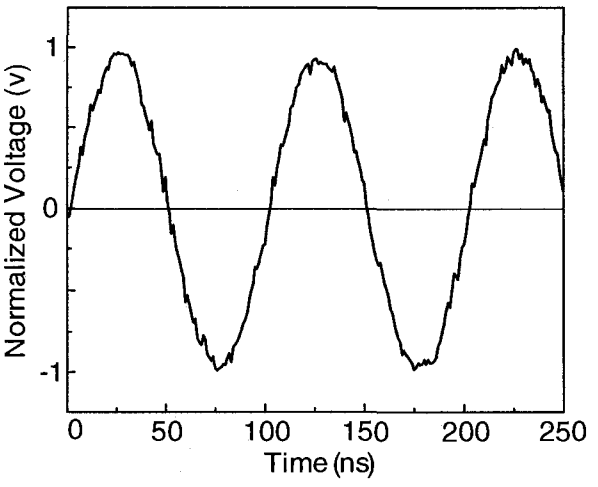

(a)

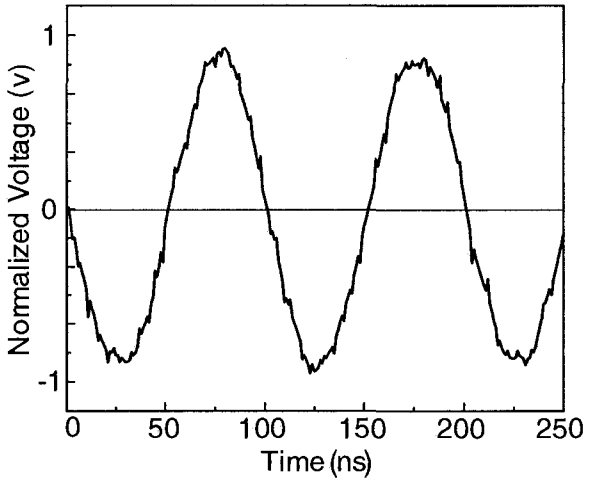

(b)

Fig. 2.4. Generation of out-of-phase microwave signals based on XPolM. (a) The inverted microwave signal along the y-axis and (b) the non-inverted microwave signal along the x-axis.

As can be seen, the two microwave signals are out of phase, corresponding to the inverted and non-inverted signals. This experiment confirms that the microwave signal carried by the pump is transferred to the two orthogonal polarization modes of the probe, with one being inverted and the other non-inverted. The detection of the two out-of-phase microwave signals with a proper time delay difference would realize a microwave bandpass filter with a positive and a negative coefficient.

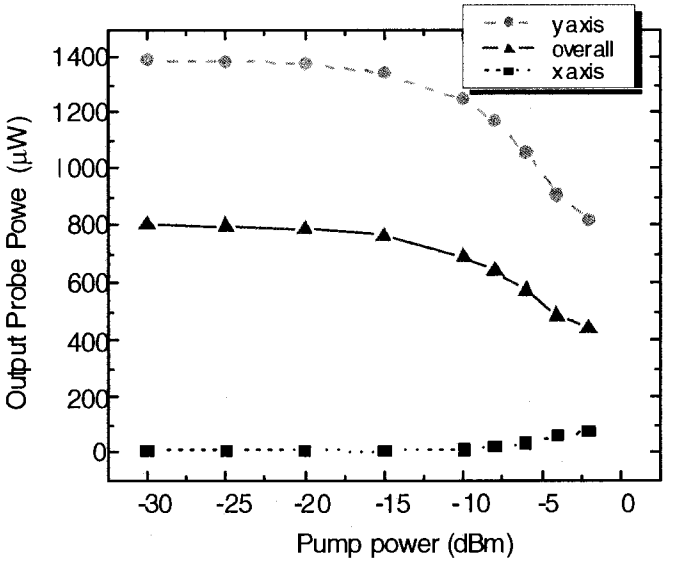

Fig. 2.5. Measured static output power of the probe light versus the input power of the pump light (-●-: y-axis probe power; -▲-: overall probe power; ··■··: x-axis probe power).

We then investigate the XPolM and the XGM in the SOA, which is performed by measuring the powers of the probe along the x- and y-axes at the output of the BPF while increasing the power of the pump from -30 dBm to -2 dBm. In the measurement, the input probe power is set at -5 dBm. The probe powers at the output of the BPF along the x- and y-axes are measured using a tunable linear polarizer and an optical power meter. When the input pump power is -30 dBm, it is too low to generate XPolM. Therefore, the probe polarization state is not altered, and all the probe power emits along the y axis. By adjusting the tunable polarizer to make its transmission axis parallel to the x axis, no probe power would be measured. We then increase the pump power. Due to the XPolM, the polarization direction of the probe beam is rotated, leading to the increase of the probe power along the x axis. As can be seen from Fig. 2.5, the power is increased from 0 to 76 μW. The change of the probe power along the x axis, which is induced by the XPolM, is proportional to the change of the pump power; therefore it carries the non-inverted signal of the pump. On the other hand, to measure the probe power along the y axis, the polarizer is adjusted to make its transmission axis parallel to the y axis, when the input pump power is -30 dBm. The increase of the pump power leads to the decrease of the probe power along the y axis; therefore it carries the inverted signal of the pump. Again, as can be seen from Fig. 2.5, the power is reduced from 1390 μW to 820 μW, with a power difference of 570 μW, which is much larger than

the non-inverted power change of 76 μW along the x axis. To measure the power change due to the XGM, we remove the tunable polarizer. If there is no XGM, although the probe powers along the x- and y-axes are increasing and decreasing, they are exactly complementary, therefore no power changes to the overall probe power would be caused by the XPolM. So the change of the probe power is only caused by the XGM. It can be seen from Fig. 2.5, the probe power is reduced from 799 μW to 440 μW. Since the XGM would equally affect the probe powers along the x- and y-axes, and the trend of the power change due to the XGM is the same as the XPolM-induced inverted signal along the y axis, the overall probe power decrease along the y axis is further enhanced. On the contrary, the overall probe power increase along the x-axis, say, the XPolM-induced non-inverted signal, is reduced.

The ratio between the two coefficients can be obtained by calculating the ratio between the power differences along the y axis and the x axis.

$$R = \frac{\left|P_{inv} - P_{0inv}\right|}{\left|P_{non-inv} - P_{0non-inv}\right|} = \frac{\left|\Delta P_{inv}\right|}{\left|\Delta P_{non-inv}\right|} \tag{2.4}$$

where ΔP_{inv} and $\Delta P_{non-inv}$ are the power difference with respect to the initial power level for the inverted signal along the y-axis and the non-inverted signal

along the x-axis, respectively. From Fig. 2.5, ΔP_{inv} = 570 μw, $\Delta P_{non-inv}$ = 76 μw, so the ratio of the two signals is equal to 7.5.

Due to the XGM, the ratio between the coefficients is large, so the impact of the XGM should be suppressed as much as possible. In order to investigate the relationship between the ratio of the coefficients and the power of the pump, we fix the power of the probe at -6.29 dBm, and increase the power of the pump beam from -10 to -2 dBm. Fig. 2.6 (solid line) shows the ratios of the two coefficients under different level of pump power. It can be seen that the ratio decreases from 39.7 to 9.1 when the pump power is increased. Obviously, keeping the power of the pump at a relatively high level is an effective way to reduce the impact of the XGM.

To study the impact of the probe power on the ratio, a similar experiment is performed. This time, we fix the probe power at -3.3 dBm, while increasing the pump power from -10 to -2 dBm. The experimental result is again shown in Fig. 2.6 (dotted line). With the increase of the pump power, the ratio of the coefficients decreases from 4.6 to 4. Compared with the previous experiment, the ratio is decreased dramatically with the increase of the probe power. Therefore, using a relatively high probe power is another way to reduce the impact of the XGM. Theoretically, we can further increase the probe power to

get a smaller coefficient ratio; however, to avoid damaging the SOA, the probe power cannot be increased without limit.

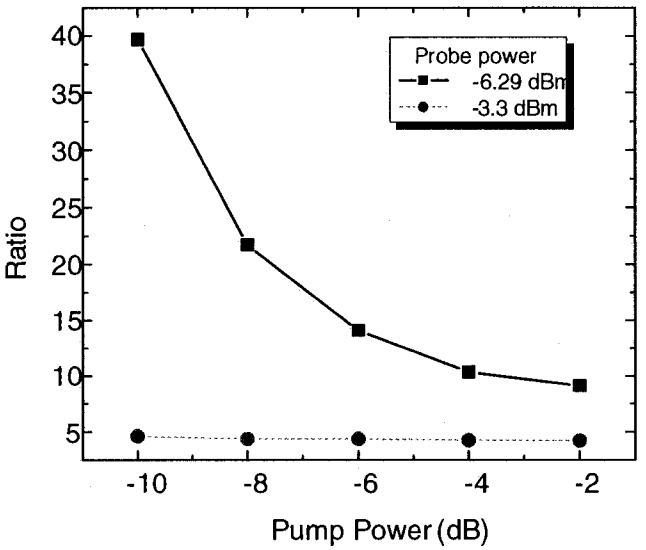

Fig. 2.6. The ratio between the two coefficients at different level of pump power, with the probe power fixed at -6.29 dBm and -3.3 dBm, respectively.

To further reduce the ratio, we propose to incorporate a tunable linear polarizer in the system after the Hi-Bi fiber. By properly adjusting the polarization axis of the tunable polarizer, we get two out-of-phase microwave signals with identical powers, as can be seen from Fig. 2.4.

Finally, we investigate the frequency response of the microwave filter. To do so, the VNA is operated to sweep the modulating frequency from 45 MHz to

20 GHz, while keeping the microwave power constant. The filter transfer function when the coefficient ratio is 1 by adjusting the transmission axis of the tunable polarizer is shown as the solid line in Fig. 2.7. As can be seen, the filter is a bandpass filter with the first resonance peak located at 8.85 GHz. The FSR is measured to be 17.6 GHz, corresponding to a time delay difference of 57 ps. The notch rejection level is 33.6 dB. The dotted curve in Fig. 2.7 shows a frequency response corresponding to a coefficient ratio of 4. The reconfigurability is demonstrated.

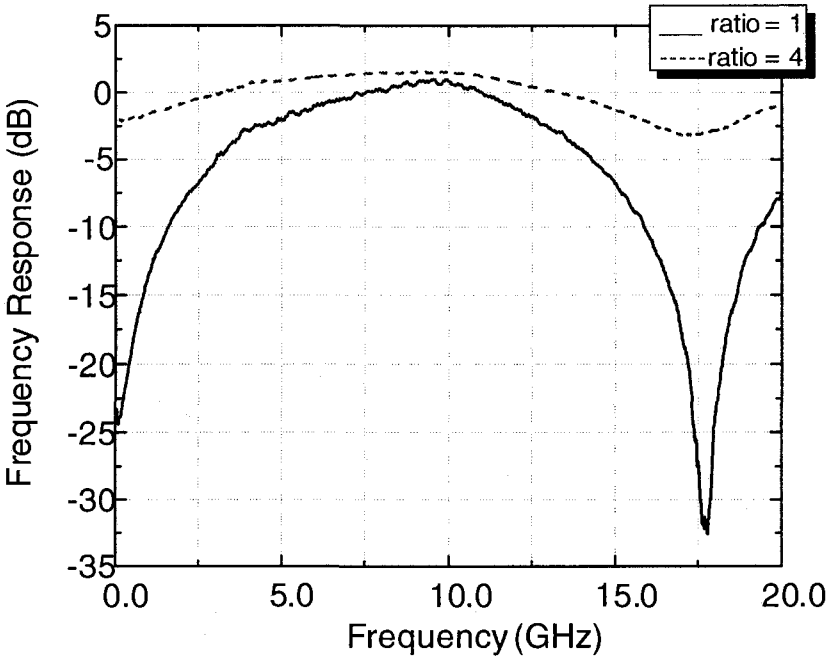

Fig. 2.7. Measured frequency response of the all-optical microwave bandpass filter corresponding to different ratios of the positive and negative coefficients (solid: ratio = 1, dotted: ratio = 4).

One added advantage of the SOA-based XPolM over the HNLF-based XPolM is that the gain of the SOA can compensate for the insertion loss of the system. The over insertion loss of the system is about 20 dB, which is completely compensated by the gain of the SOA, as can be seen from Fig. 2.7.

In the experiment, the time delay difference is introduced by a single section of Hi-Bi fiber, therefore a two-tap filter is implemented. To implement the filter with more taps, we may use a polarization beam splitter (PBS) to separate the two polarization modes, and attenuate the stronger mode using an optical attenuator. Then the single section of Hi-Bi fiber can be replaced by two sections of Hi-Bi fiber, with the length of the second section twice that of the first one, and the azimuth angle between the fast axis of the two sections is adjusted be to 45°. Therefore, each polarization mode in the first section of Hi-Bi fiber will be projected into two polarization modes in the second section. As a result, a four tap microwave filter with two negative coefficients and two positive coefficients can be obtained [38]. In the same way, more taps can be achieved by using more sections of Hi-Bi fiber.

2.3 Summary

We have proposed and demonstrated a novel all-optical microwave bandpass filter with negative coefficients based on the XPolM in an SOA. A two-tap microwave filter with one negative and one positive coefficient was experimentally demonstrated. The key component in the filter was the SOA, which was used to achieve the XPolM. To make the filter reconfigurable, we incorporate a tunable polarizer in the system after the Hi-Bi fiber. By tuning the polarization axis of the polarizer, the filter coefficients can be adjusted. Compared with the approach using a long nonlinear fiber to achieve XPolM, the filter here has a smaller size and has the potential for integration using photonic integrated circuit technology. The experimental results showed that the filter could operate stably at room temperature without suffering from the optical interferences.

Chapter 3

TUNABLE PHOTONIC MICROWAVE BANDPASS FILTER BASED ON PHASE MODULATOR AND LINEARLY CHIRPED FIBER BRAGG GRATINGS

In Chapter 2, we have proposed and demonstrated a photonic microwave bandpass filter with negative coefficients based on the XPolM in an SOA. Recently, it was demonstrated that the phase modulation to intensity modulation conversion (PM-IM) would have a frequency response with a notch at dc. The baseband resonance of a conventional photonic microwave filter with all positive coefficients would be eliminated by the PM-IM notch [53]-[54], leading to a bandpass-equivalent filter. Although the filters in [53]-[54] are bandpass filters, they have all positive coefficients which lead to the filter responses with a non-flat top and high sidelobes. To design a bandpass filter with a frequency response that has a flat top and low sidelobes, true bandpass filter with negative coefficients should be implemented. In [37], we proposed a true bandpass filter. The negative coefficients were generated by reflecting the phase-modulated optical carriers from linearly chirped fiber

Bragg gratings (LCFBGs) with group-delay responses having positive or negative slopes. The phase-modulated signals were converted to intensity-modulated signals at the LCFBGs with phase inversion, leading to the generation of negative coefficients.

On the other hand, it is highly desirable that the microwave filters be tunable. Various configurations have been reported for the implementation of tunable optical microwave filters [27] [55]-[59]. In general, the tunability can be achieved by using variable optical delay lines [55] [56], by tuning optical wavelengths combined with dispersive optical devices having fixed chromatic dispersions [27] [57] [58], or by tuning chromatic dispersions combined with fixed optical wavelengths [59]. The filters demonstrated in [27] [55]-[59] are tunable microwave filters, but all with positive coefficients only, making them function as lowpass filters.

In this chapter, we propose a novel photonic microwave bandpass filter with negative coefficients that is tunable. In the proposed filter, the microwave signal is modulated on an optical carrier using an optical phase modulator. The positive and negative coefficients are generated through optical phase-modulation to intensity-modulation (PM-IM) conversion by reflecting the phase-modulated optical carrier from LCFBGs with group-delay responses

having positive or negative slopes. The tunability is realized by changing the wavelength of the optical carrier which is reflected at different physical locations in the LCFBGs, leading to the generation of different time delays. Therefore, the LCFBGs in the proposed filter have two functions, to generate positive and negative coefficients and to make the filter tunable.

This chapter is organized as follows. In Section 3.1, the generation of positive and negative coefficients based on PM-IM conversion using LCFBGs is discussed; then a tunable microwave bandpass filter with positive and negative coefficients implemented based on PM-IM conversion using LCFBGs is proposed and analyzed. In Section 3.2, experimental implementation of a two-tap tunable microwave bandpass filter using two LCFBGs is presented. A conclusion is drawn in Section 3.3.

3.1 Principles

3. 1. 1 Generation of positive and negative coefficients based on PM-IM conversion using LCFBGs

The schematic diagram illustrating the generation of positive and negative coefficients based on PM-IM conversion using LCFBGs is shown in Fig. 3.1.

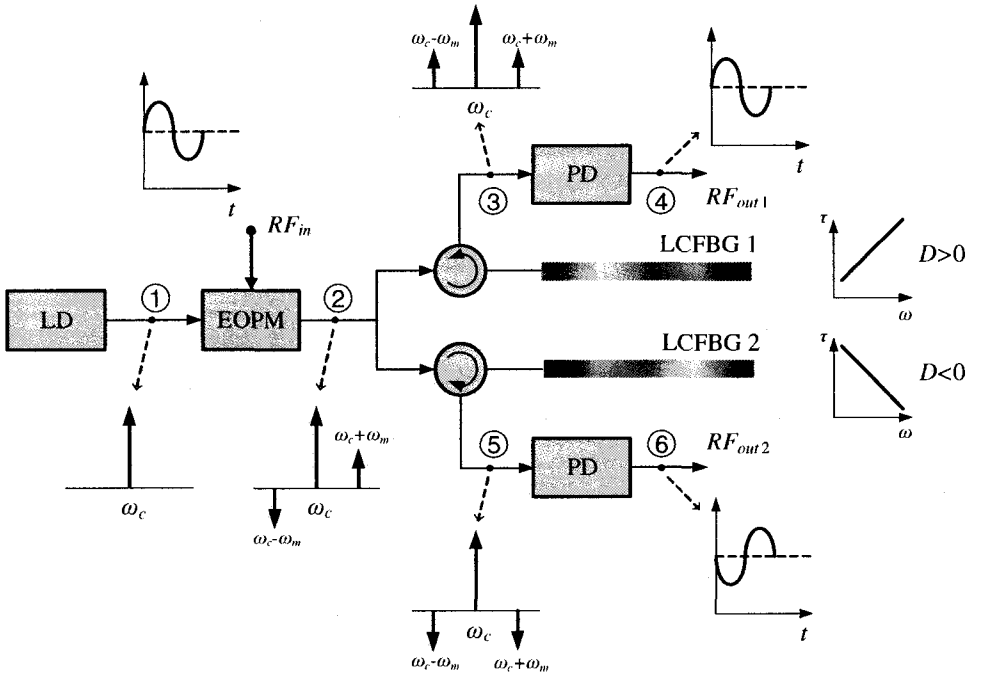

Fig. 3.1. Generation of positive and negative coefficients based on PM-IM conversion using LCFBGs. LD: laser diode; EOPM: electro-optic phase modulator; PD: photodetector.

In the system, the electro-optic phase modulator (EOPM) is driven by a microwave signal. Under small signal condition, the phase-modulated optical field $E(t)$ can be expressed as [60]

$$E(t) = J_0(m_p V)\cos(\omega_c t) + J_1(m_p V)\cos\left[(\omega_c + \omega_m)t + \frac{\pi}{2}\right]$$

$$-J_1(m_p V)\cos\left[(\omega_c - \omega_m)t - \frac{\pi}{2}\right] \tag{3.1}$$

where $J_n(m_p V)$ is the nth-order Bessel function of the first kind, m_p is the phase modulation index, V is the amplitude of microwave modulating signal, ω_c is the angular frequency of the optical carrier, and ω_m is the angular frequency of the microwave modulating signal. It can be seen that the two sidebands of the phase-modulated signal at the output of the EOPM are π out of phase (point ② in Fig. 3.1). If this phase-modulated optical signal is directly applied to a PD, the beating between the carrier and the upper sideband will exactly cancel the beating between the carrier and the lower sideband. Therefore, no microwave signal other than a dc can be obtained at the output of the PD. However, as shown in Fig. 3.1, if the phase-modulated optical signal passes through a LCFBG, the chromatic dispersion of the LCFBG will change the phase relationships of the carrier and the two sidebands. The optical field at the output of the LCFBG is given by [61]

$$E(t) = J_0 \cos(\omega_c t + \theta_0) + J_1 \cos\left[(\omega_c + \omega_m)t + \frac{\pi}{2} + \theta_{+1}\right] - J_1 \cos\left[(\omega_c - \omega_m)t - \frac{\pi}{2} + \theta_{-1}\right] \tag{3.2}$$

where θ_0, θ_{+1} and θ_{-1} are the phase shifts of the carrier, the upper sideband and the lower sideband, respectively. The phase shift induced by the dispersion of the LCFBG can be generally written as [61]

$$\theta = z\beta(\omega_c) + z\beta'(\omega_c)(\omega - \omega_c) + \frac{1}{2} \cdot z\beta''(\omega_c)(\omega - \omega_c)^2 + \cdots \tag{3.3}$$

where z is the travel distance, β is the propagation constant, β' and β'' are the first- and second-order derivatives of β, respectively. Since the group delay response of an LCFBG is linear, the third- or higher-order derivatives of β can be ignored. Thus, the group delay can be written as [61]

$$\tau(\omega) = \frac{d\theta}{d\omega} = z\beta'(\omega_c) + z\beta''(\omega_c)(\omega - \omega_c) \tag{3.4}$$

The group delay of the optical carrier is the first term of the right side of Eq. (3.4), which is given by $\tau_0 = z\beta'(\omega_c)$. The chromatic dispersion of the LCFBG is the first-order derivative of the group delay, which is given by $D = z\beta''(\omega_c)$. Therefore, the phase shifts of the carrier, the upper sideband and the lower sideband can be expressed as

$$\theta_0 = z\beta(\omega_c),\ \theta_{+1} = z\beta(\omega_c) + \tau_0\omega_m + \frac{1}{2}D\omega_m^2,\ \theta_{-1} = z\beta(\omega_c) - \tau_0\omega_m + \frac{1}{2}D\omega_m^2 \tag{3.5}$$

Obviously, the chromatic dispersion of the LCFBG will change the phase relationships of the carrier and the two sidebands. Therefore, the two

sidebands of the phase-modulated signal can be partially or totally in phase after experiencing the chromatic dispersion. When the optical signal after the dispersion is applied to the PD, the microwave modulating signal can thus be recovered. As a result, the PM signal is converted to an IM signal. Mathematically, the electrical field of the recovered microwave signal is given by

$$E_{RF}(t) \propto \sin\left(\frac{\pi D \lambda_c^2 f_m^2}{c}\right) \cdot \cos(\omega_m t + \theta) \tag{3.6}$$

where D is the chromatic dispersion of the LCFBG, λ_c is the wavelength of the optical carrier, f_m is the microwave modulating frequency, c is the optical velocity in free space, and θ is the phase delay of the recovered microwave signal, which is also determined by D and f_m [60].

As shown in Fig. 3.1, two LCFBGs are employed to generate a positive and a negative coefficients. To do so, the two LCFBGs are connected in opposite directions. Assume that LCFBG1 is connected such that its chromatic dispersion $D = \partial\tau / \partial\omega > 0$, where τ is the group delay. In this case, the higher optical frequency component will experience more phase shift due to the positive chromatic dispersion. For a specific microwave frequency, say ω_m, the phase relationships of the two sidebands and the carrier may be changed to totally in phase (point ③ in Fig. 3.1) after the chromatic

dispersion, thus the PM signal is converted to an IM signal, which can be detected by the PD (point ④ in Fig. 3.1). On the other hand, if LCFBG2 is connected such that its chromatic dispersion $D = \partial\tau / \partial\omega < 0$, the lower frequency component would experience more phase shift. After the chromatic dispersion, the two sidebands will be in phase, but are π out of phase with respect to the optical carrier (point ⑤ in Fig. 3.1). After the photodetection at the PD, the beating between the carrier and the two sidebands will recover the microwave modulating signal, but with a phase difference of π (point ⑥ in Fig. 3.1). The use of the two out-of-phase microwave signals with a proper time delay difference between them would achieve a two-tap microwave filter with one positive and one negative coefficient.

The phase inversion can also be easily explained mathematically. As can be seen from Equation (3.2), if the sign of the chromatic dispersion D is changed, the sign of the recovered microwave signal will also be changed, because $\sin\left(\pi D \lambda_c^2 f_m^2 / c\right)$ is an odd function of D.

3. 1. 2 Tunable photonic microwave bandpass filter based on PM-IM conversion

Based on the above analysis, we propose a tunable photonic microwave bandpass filter based on PM-IM conversion using LCFBGs. To demonstrate the concept, only two LCFBGs are used. Therefore, the filter is a two tap filter. The filter can be extended to multiple taps, if more LCFBGs are used. The configuration of the proposed filter is shown in Fig. 3.2. In the system, a lightwave from a tunable laser source (TLS) is phase-modulated by an EOPM. A polarization controller (PC1) is connected between the TLS and the EOPM to align the polarization direction of the laser beam with the principle axis of the EOPM, to minimize the polarization-dependent loss. The phase-modulated optical signal is then sent to two LCFBGs through an optical circulator and an optical coupler. The two LCFBGs are connected in such a way that one has a positive dispersion and the other has a negative dispersion. The spacing d between the two LCFBGs, shown in Fig. 3.2, determines the smallest time delay difference between the two taps. When the wavelength is tuned, the time delay difference will be changed, the free spectral range (FSR) of the filter is thus changed. The filter is tunable.

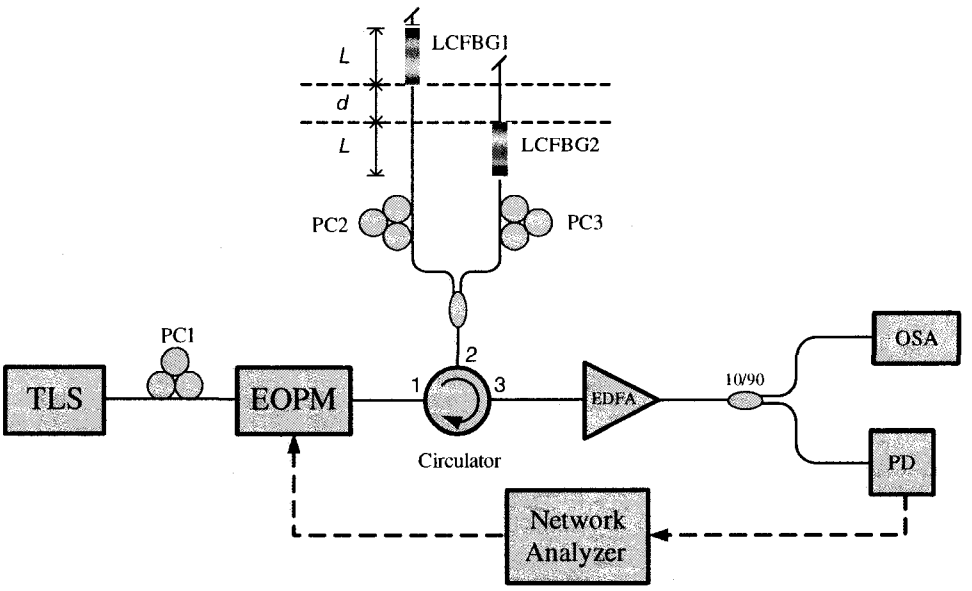

Fig. 3.2. Experimental setup of the proposed microwave bandpass filter

Since the two optical signals reflected by the two LCFBGs are from the same laser source, when they recombine at the PD, optical interference would happen. To eliminate the optical interference, in the proposed filter we use two PCs (PC2 and PC3) to make the two reflected optical signals orthogonally polarized. Another solution to avoid optical interference is to use an optical source that has a low coherence, such as a sliced ASE (Amplified Spontaneous Emission) or sliced SLED (Superluminescent Light Emitting Diode) source.

Assuming the reflection coefficients of the LCFBGs are identical, the frequency response of the proposed filter is then given by

$$H(\omega) \propto \sum_{n=1}^{2} \sin\left(\frac{\pi D_n \lambda_c^2 f_m^2}{c}\right) \exp[j\omega_m (n-1)\Delta\tau] \tag{3.7}$$

where $\Delta\tau$ is the time delay between the two taps, which is given by

$$\Delta\tau = \frac{2n_{eff}}{c} \cdot \Delta L = \frac{2n_{eff}}{c} \cdot \left(l_0 + \frac{2(\lambda_0 - \lambda_c)L_g}{\Delta\lambda_g}\right) \tag{3.8}$$

where n_{eff} is the effective refractive index of the gratings, L_g is the length of the LCFBGs, ΔL is the distance between the reflection points of the gratings, which is a function of the carrier wavelength, l_0 is the distance between the reflection points at the central wavelength λ_0, and $\Delta\lambda_g$ is the bandwidth of the LCFBG. Assume that the lengths and the chirp rates of the two gratings are identical, and the bandwidth of each grating is less than 1 nm, then $\lambda_c^2 \approx \lambda_0^2$, (3.7) can now be rewritten as

$$H(\omega) \propto \underbrace{\sin\left(\frac{\pi D \lambda_0^2 f_m^2}{c}\right)}_{H_1(\omega)} \cdot \underbrace{\left\{1 - \exp\left[j\omega_m \frac{2n_{eff}}{c} \cdot \left(l_0 + \frac{2(\lambda_0 - \lambda_c)L_g}{\Delta\lambda_g}\right)\right]\right\}}_{H_2(\omega)} \tag{3.9}$$

The frequency response of the filter is the multiplication of two frequency responses $H_1(\omega)$ and $H_2(\omega)$. $H_1(\omega)$ is the frequency response of the PM-IM conversion using a LCFBG, and $H_2(\omega)$ is the frequency response of an ideal two-tap bandpass filter with one positive and negative coefficient. The FSR of the filter can be given

$$FSR = \frac{1}{\Delta\tau} = \frac{c}{2n_{eff}} \frac{1}{\left(l_0 + \frac{2(\lambda_0 - \lambda_c)L_g}{\Delta\lambda_g} \right)} \tag{3.10}$$

By tuning the wavelength λ_c of the optical carrier, the FSR can be changed. The filter is thus tunable.

Note that the proposed filter has only two taps, which can be extended to a multi-tap microwave filter by adding more TLS and more LCFBGs acting as more taps, as shown in Fig. 3.3.

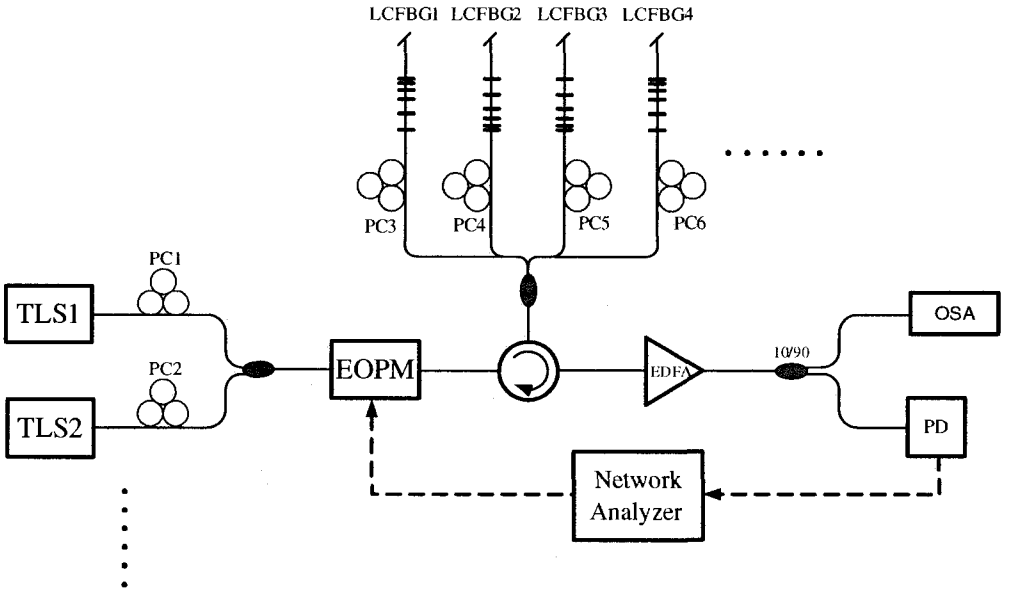

Fig. 3.3. Multi-tap tunable photonic microwave bandpass filter using multiple TLSs.

The lightwave from TLS1 will be reflected by LCFBG1 and LCFBG2, which have the same chirp rates and opposite dispersions. The lightwave from TLS2 will be reflected by LCFBG3 and LCFBG4, also with same chirp rates and opposite dispersions. The chirp rates of LCFBG3 and LCFBG4 are equal to 3 times that of LCFBG1 and LCFBG2. Assuming the wavelengths of the TLSs are first tuned such that the reflection points are located at the center of each grating, as shown in Fig. 3.4(1). By changing the wavelengths of the TLSs, the reflection points will shift along the gratings. The shift distance is determined by the chirp rate, and the shift direction is determined by the polarity of the dispersion, as shown in Fig. 3.4(2). As a result, the optical path difference between any two taps will be 4L (because of the reflection). Two more polarization controllers (PC5 and PC6) are inserted to make the reflected optical signals from LCFBG3 and LCFBG4 orthogonally polarized. In addition, since TLS1 and TLS2 are incoherent sources, the optical interference is eliminated in the system. By adding more TLSs and LCFBGs, the filter can be extended to more taps.

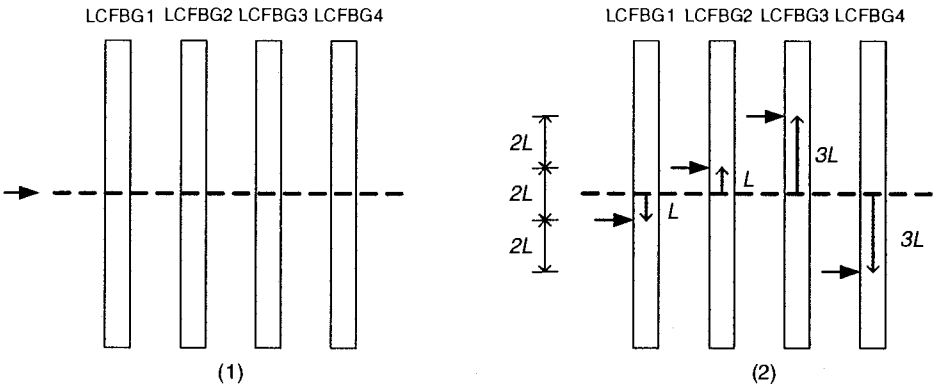

Fig. 3.4. Shift of the reflection points along the LCFBGs

Another method to extend the proposed approach to multi-tap tunable filter is to use an optical source with low coherence, such as a sliced ASE or sliced SLED source. The configuration is shown in Fig. 3.5.

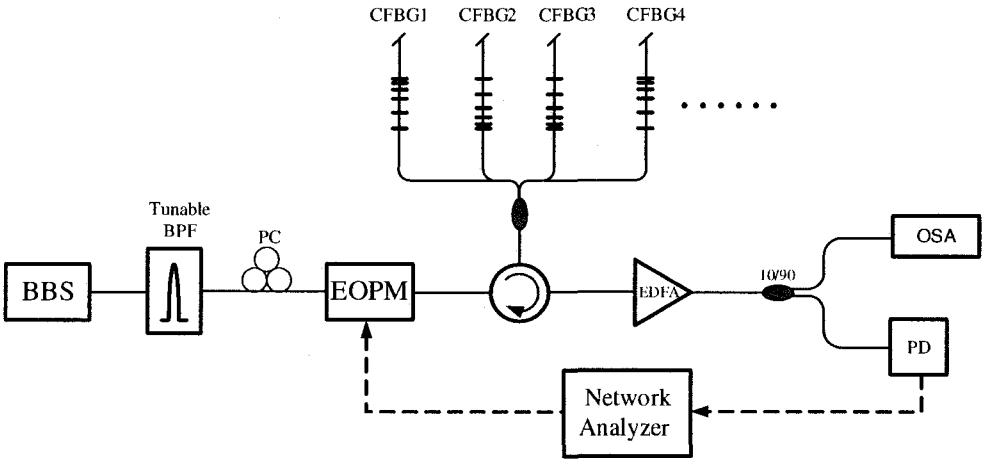

Fig. 3.5 Multi-tap tunable photonic microwave bandpass filter using broadband source. BBS: broadband source; BPF: bandpass filter.

In this case, the PCs to maintain the orthogonality between the two reflected lightwaves from one CFBG are not needed since no optical interference would be generated when using a broadband source with low coherence. The tunability is realized by simply tuning the wavelength of the tunable optical filter. The chirp rates of the LCFBGs for these two methods should be carefully designed to ensure that the time-delay differences between any two adjacent taps are identical. The insertion loss due to a large number of taps could be compensated by incorporating an optical amplifier in the filter before photodetection.

3.2 Experiments and discussions

An experimental setup based on the configuration in Fig. 3.2 was built. A TLS with a typical linewidth of 150 kHz was used as the light source. Two LCFBGs were fabricated in hydrogen-loaded standard single mode fiber using phase mask technique. The lengths of the two LCFBGs were 8 cm. The chromatic dispersions of the LCFBGs were 1344 ps/nm and -1370 ps/nm.

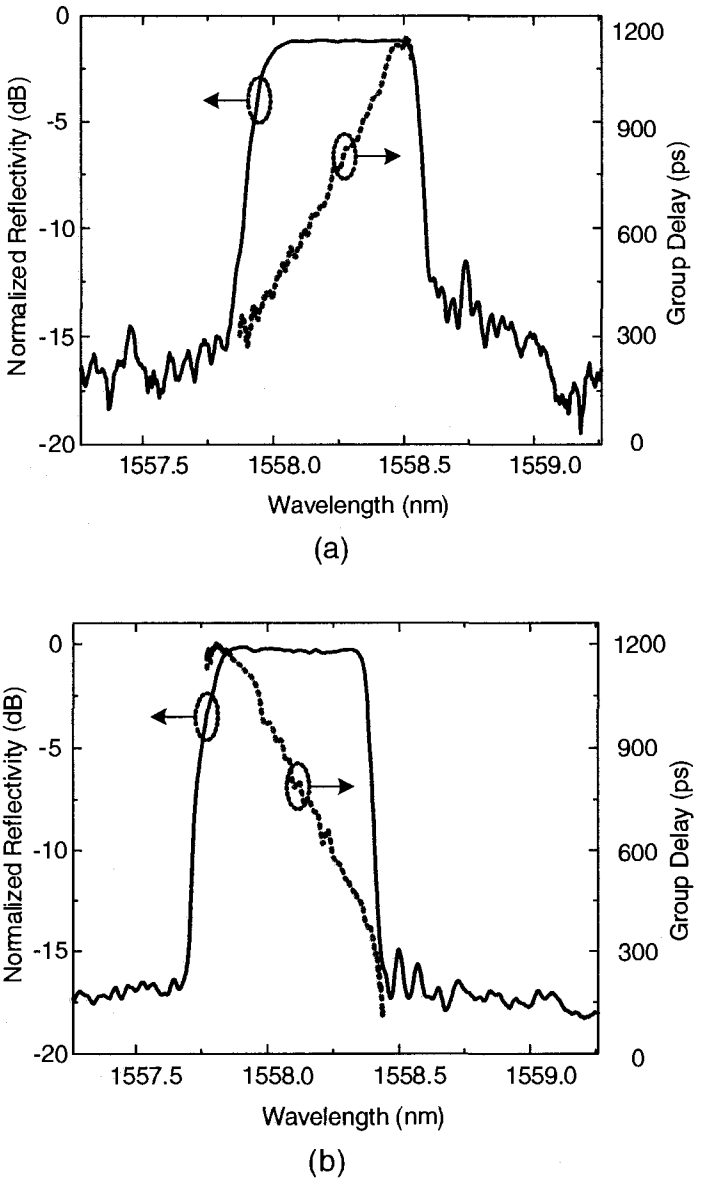

Fig. 3.6. Measured reflectivity and group delay responses of (a) LCFBG1 and (b) LCFBG2

The reflection spectrum and the group delay response of the two LCFBGs are shown in Fig. 3.6. As can be seen, the reflection spectrums of the two gratings

have an overlap of about 0.6 nm. By tuning the wavelength of the TLS within this overlapping region, two optical signals will be reflected by the two gratings, with different time delay difference.

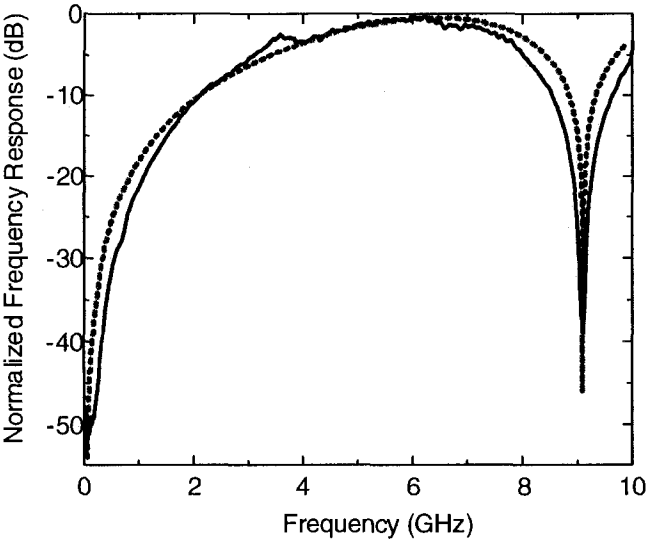

Fig. 3.7. The measured (solid curve) and the simulated (dotted curve) frequency response of the PM-IM conversion based on a LCFBG.

Before we measure the frequency response of the two-tap microwave filter, we first investigate the PM-IM conversion using an LCFBG. To do so, we disconnect LCFBG2, and measure the frequency response of the system with only one grating (LCFBG1) connected. The frequency response is measured using a vector network analyser (VNA), which is shown in Fig. 3.7 (solid curve). As can be seen a deep notch is observed at dc. A theoretical frequency

response calculated based on (3.2) is also shown in the figure (dotted curve). An excellent agreement is observed between the experimental result and the theoretical prediction.

Based on (3.5), the overall frequency response of the filter is the multiplication of $H_1(\omega)$ and $H_2(\omega)$. Since the bandwidth of $H_1(\omega)$ is very wide, its impact on the overall frequency response can be negligible, especially for a microwave bandpass filter with many taps (narrow passband).

Then, we reconnect LCFBG2 to the system. This filter is now a two-tap filter with one positive and one negative coefficient. The filter frequency response is again measured using the VNA. To demonstrate the tunability, the wavelength of the TLS is tuned at four different wavelengths. The frequency responses at 1557.83, 1557.99, 1558.20 and 1558.39 nm are shown in Fig. 3.8 (solid curve). The dotted line shows the frequency response of an ideal two-tap microwave filter with one positive and one negative coefficient with a time delay difference of 879.5 ps, 458.7 ps, 302.1 ps and 219.8 ps. The FSRs for the four different measurements are 1.14, 2.18, 3.31 and 4.55 GHz, corresponding to a distance between the two reflection points of 17.59, 9.17, 6.04, and 4.4 cm, or a time delay difference of 879.5 ps, 458.7 ps, 302.1 ps, and 219.8 ps.

The tunable range can be further increased if the bandwidths of the two LCFBGs are increased.

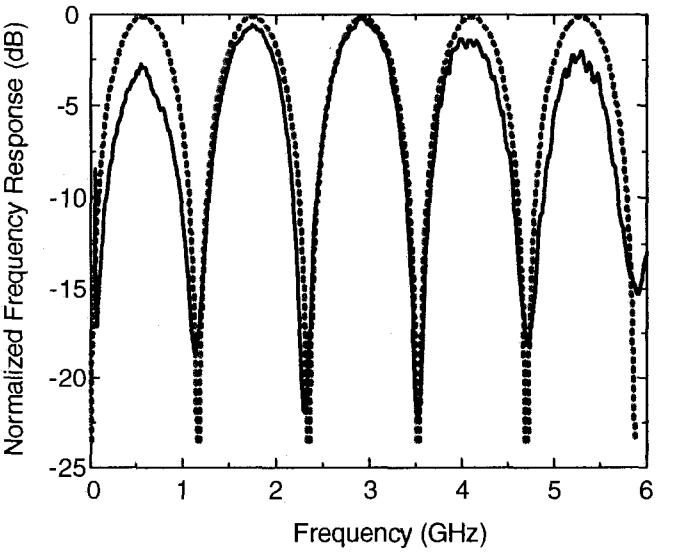

(a)

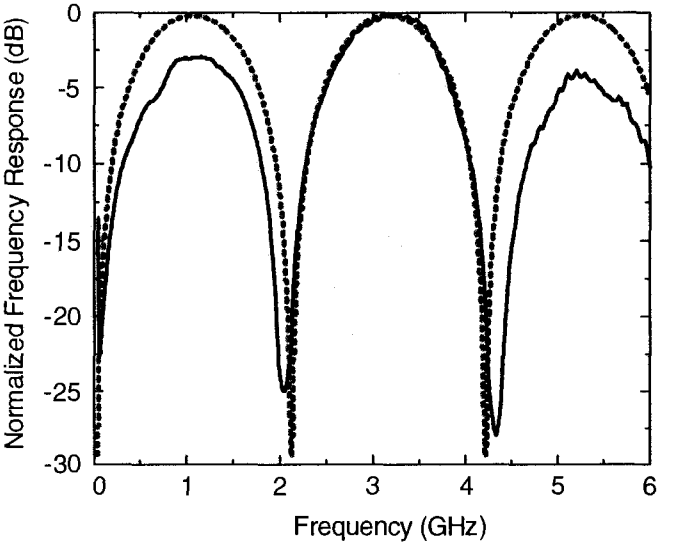

(b)

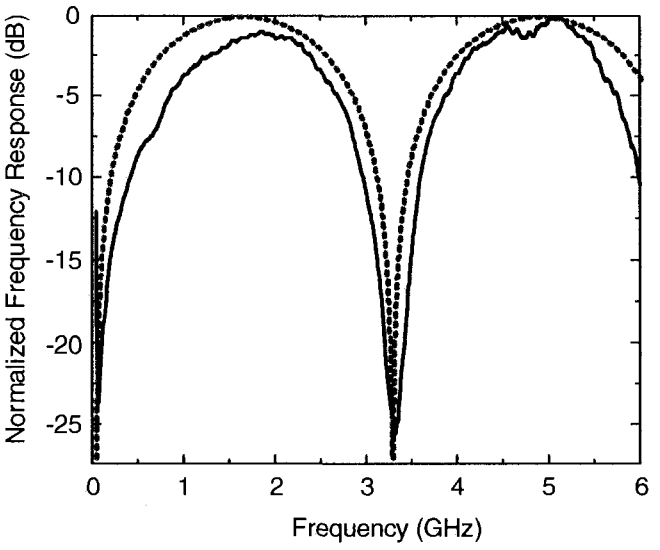

(c)

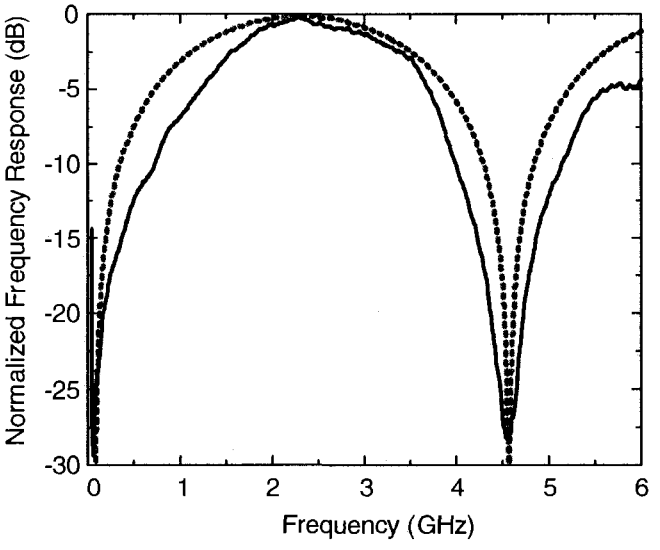

(d)

Fig. 3.8. The measured frequency response (solid curve) and the ideal frequency response (dotted curve) of a two-tap bandpass microwave filter with one positive and one negative coefficient. The FSR is (a) 1.14 GHz, (b) 2.18 GHz, (c) 3.31 GHz, and (d) 4.55 GHz.

3.3 Summary

A novel continuously tunable optical microwave bandpass filter with negative coefficient implemented based on PM-IM conversion using LCFBGs was proposed and experimentally demonstrated. The positive and negative coefficients were generated based on PM-IM conversion by reflecting the phase-modulated optical carriers from the LCFBGs with positive or negative dispersions. The tunability was realized by tuning the wavelength of the optical carrier. The major advantage of this filter is that it has a simple structure with continuous tunability and large tunable range. A two-tap microwave bandpass filter with an FRS tunable from 1.14 to 4.55 GHz was experimentally demonstrated.

Chapter 4

TUNABLE PHOTONIC MICROWAVE FILTER WITH COMPLEX COEFFICIENTS

In Chapter 2 and Chapter 3, we proposed two photonic microwave bandpass filters with negative coefficients. For many applications, such as scanning receivers and microwave test equipments, it is highly desirable that the microwave filters be tunable. Various configurations have been reported for the implementation of tunable optical microwave filters [56] [27] [57] [59]. The tunability is usually achieved by adjusting the time delay difference, which can be realized by directly using tunable optical delay lines [56], by using wavelength tunable light sources in combination with a dispersive optical device [27] [57], or by using a dispersion-tunable device in combination with fixed wavelength light sources [59]. However, the change of the time delay difference would lead to the changes of the free spectral range (FSR), which results in the change of 3-dB bandwidth as well as the entire shape of the filter frequency response. For many applications, it is highly desirable that only the center frequency of the passband or stop-band be changed while keeping the shape of the frequency response unchanged. A

solution to this problem is to use a photonic microwave filter with complex coefficients.

Two configurations have been recently reported in [40] [41] for the implementation of tunable microwave filters with complex coefficients. In [40], the complex coefficient was generated in a system using three optical attenuators and two microwave couplers. The use of optical attenuators achieves only positive coefficients, adjustable between 0 and 1, which limits the RF phase shift from 0 to 180° or a tunable range of half the FSR [40]. In [41], a tunable photonic microwave filter with complex coefficient that has a tunable range up to one FSR was demonstrated. In the system, the complex coefficient was generated by changing the phase of the microwave signal, which was realized based on a combined use of optical single-sideband modulation (SSB) and stimulated Brillouin scattering (SBS).

In [41], to stimulate the SBS, a 20-km single mode fiber was used, which makes the system bulky. To avoid using a long optical fiber, we propose a novel tunable photonic microwave filter with a very simple structure [62]. In the proposed filter, the complex coefficient is generated based on a wideband tunable optical RF phase shifter [63] [64], in which the phase of the RF signal can be shifted by simply adjusting the bias voltages applied to two electro-

optic intensity modulators (IMs), with the phase shift kept constant over the microwave spectral region of interest. A two-tap photonic microwave filter with one tunable complex coefficient is experimentally demonstrated.

4. 1 Principle

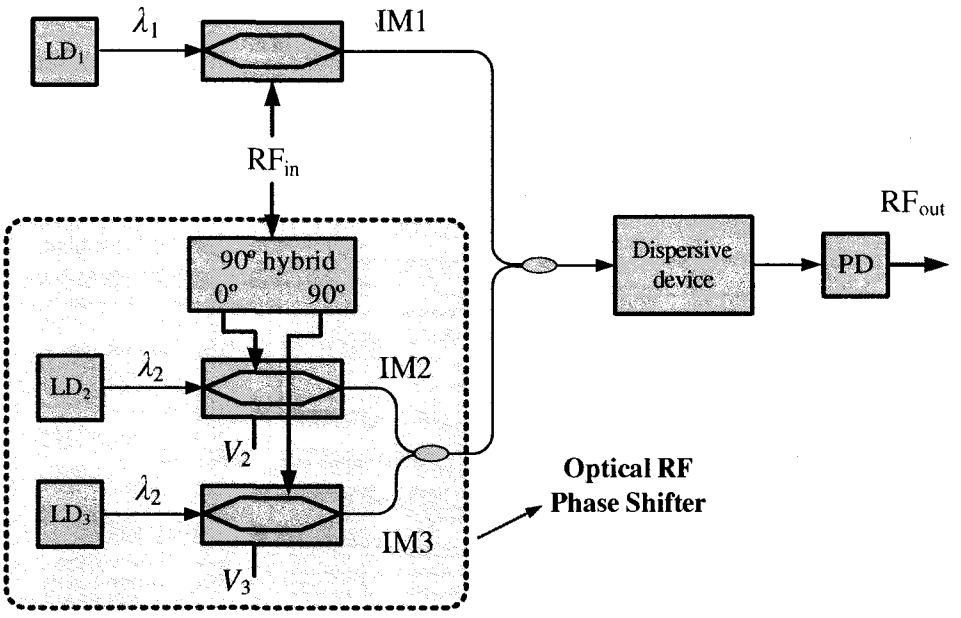

Fig. 4.1. Generation of a complex coefficient based on optical RF phase shifter.

The schematic diagram illustrating the generation of a complex coefficient based on a wideband tunable optical RF phase shifter is shown in Fig. 4.1. It is

a two-tap filter with one tap having a real positive coefficient and the other tap having a complex coefficient. The real positive coefficient is generated using an intensity modulator (IM1) with an input lightwave operating at λ_1. The complex coefficient is generated by the optical RF phase shifter, shown in the dashed-line box of Fig. 4.1. In the RF phase shifter, two independent light sources both operating at the same wavelength λ_2, are sent to two intensity modulators (IM2 and IM3), which are modulated by the in-phase and the quadrature components of the microwave signal from a 90° hybrid coupler. The input optical intensities of the two intensity modulators (IM2 and IM3) are I_2 and I_3, and the bias voltages are V_2 and V_3. The output signals from the two IMs are then combined by an optical coupler. Since the two lightwaves are generated by two independent light sources, the optical interference at the optical coupler is minimized, even though they are operating at the same wavelength. If we set $I_2 = I_3 = I$ and $V_3 = V_\pi / 2 - V_2$, where V_π is the half-wave voltage of the intensity modulators, the electrical field at the output of a photodetector (PD) is given by [63]

$$E_{RF}(t) \propto J_1\left(\pi V_m / V_\pi\right) \cdot I \cdot \left[\sin\left(\omega t + \phi + \theta\right)\right] \tag{4.1}$$

where V_m is the amplitude of the microwave modulating signal, $J_1\left(\pi V_m / V_\pi\right)$ is the first-order Bessel function of the first kind, ω is the microwave frequency, ϕ is the initial phase of the microwave signal, and $\theta = \pi V_3 / V_\pi$ is

the phase shift of the microwave signal introduced by the optical RF phase shifter. As can be seen, the RF phase shift θ is a linear function of the bias voltage V_3, which is independent of the input microwave frequency, and can be easily tuned by adjusting the bias voltages. Note that the tuning of the bias voltages would lead to the change of the optical intensities at the outputs of the two IMs, which can be compensated by adjusting the optical powers of the laser sources. To eliminate the frequency-dependent phase shift, the fiber lengths from the outputs of the three IMs to the input of the optical delay line should be controlled to be identical [63].

To introduce a time delay difference between the microwave signal carried by wavelength λ_1 and the phase-shifted microwave signal carried by wavelength λ_2, a dispersive device may be used to introduce a time delay difference, as shown in Fig. 4.1. The dispersive device can be a length of dispersive fiber. To reduce the size, the dispersive fiber can be replaced by two cascaded fiber Bragg gratings (FBGs) or a single chirped FBG. The time-delayed microwave signals are then applied to the PD. The transfer function of the filter can be written as

$$H(\omega) = 1 + e^{-j\theta} \cdot e^{-j\omega\Delta\tau} \tag{4.2}$$

where $\Delta\tau$ is the time-delay difference between the two time-delayed microwave signals. As can be seen, the filter has two taps with one complex

coefficient $e^{-j\theta}$. By tuning the bias voltages applied to IM2 and IM3, the phase shift can be changed, leading to the tuning of the complex coefficient.

Note that the two-tap filter shown in Fig. 4.1 can be easily extended to a multi-tap filter by adding more optical RF phase shifters with complex coefficients or intensity modulators with real positive coefficients. The physical separation between any two adjacent FBGs or the wavelength spacing between any two adjacent wavelengths should be kept identical to maintain an identical time delay difference.

4. 2 Experiments

The proposed system was experimentally investigated. To demonstrate the concept, only a two-tap photonic microwave filter with one complex coefficient, shown in Fig. 4.2, was built. To simplify the system, the intensity modulator (IM1) in Fig. 4.2 is used to perform two functions, 1) to modulate the microwave signal on the optical carrier at λ_1, and 2) to work jointly with IM2 to form an optical RF phase shifter.

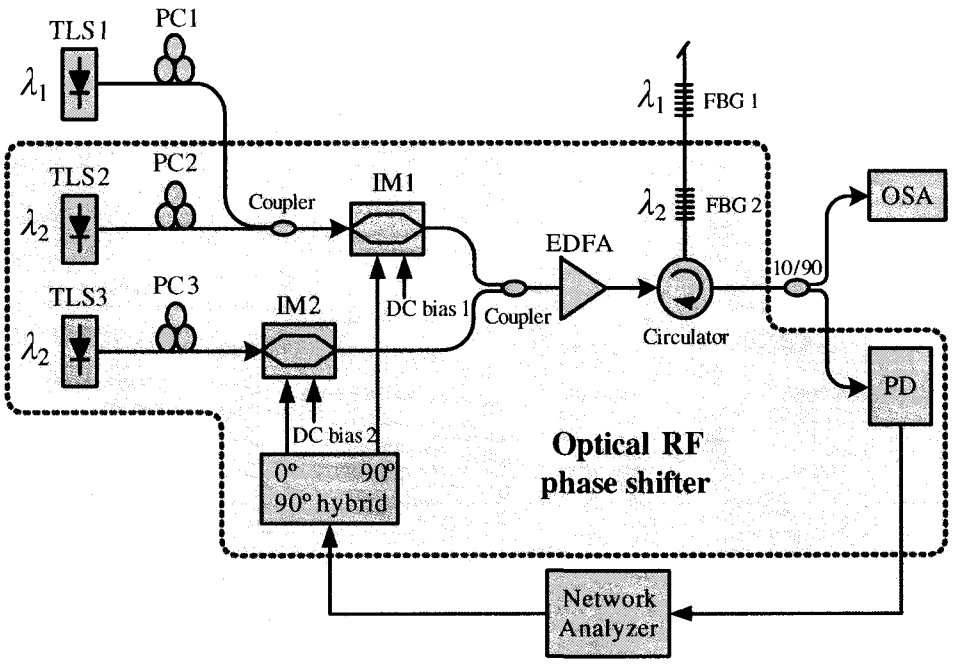

Fig. 4.2. Experimental setup of the proposed filter. TLS: tunable laser source; PC: polarization controller; and OSA: optical spectrum analyzer.

The output from a tunable laser source (TLS1) at a wavelength of $\lambda_1 = 1546.29$ nm is injected into IM1 through an optical coupler. In the optical RF phase shifter, two lightwaves from two independent tunable laser sources (TLS2 and TLS3), both at the same wavelength of $\lambda_2 = 1549.68$ nm, are sent to IM1 and IM2. The polarization controllers (PC1, PC2 and PC3) connected between the tunable laser sources and the intensity modulators are used to align the polarization directions of the lightwaves with the principle axes of the intensity modulators, to minimize the polarization-dependent loss. The

microwave signal generated by a vector network analyzer (VNA) is applied to the two IMs via a 90° hybrid coupler, with the in-phase and the quadrature components to drive IM2 and IM1, respectively. The microwave signal carried by wavelength λ_1 and the phase-shifted microwave signal carried by λ_2 are combined at an 3-dB coupler and amplified by an erbium-doped fiber amplifier (EDFA), and then time delayed by two cascaded FBGs with a time-delay difference determined by the physical separation of the two FBGs.

We first investigate the phase-shift property of the optical RF phase shifter, which is shown in the dashed-line box of Fig. 4.2. In this case, TLS1 is disconnected. By sweeping the microwave frequency, we obtain the phase shift of the recovered microwave signal, which is measured by the VNA. As can be seen in Fig. 4.3, the phase shift of the microwave signal is from -180° to 180° by adjusting the bias voltages applied to the two IMs. The tuning range of the bias voltages is 0~12 V, determined by the half-wave voltage of the IMs. The phase shift is independent of the microwave frequency. Therefore, it is possible to use this RF phase shifter to generate the complex coefficient in the photonic microwave filter with a tunable range of one FSR. The variations of the phase shifts are caused by the measurement errors, including the variations of the optical fibers and the RF cables. Using the photonic integrated circuits technology, the phase errors can be controlled to be smaller than 3° [63].

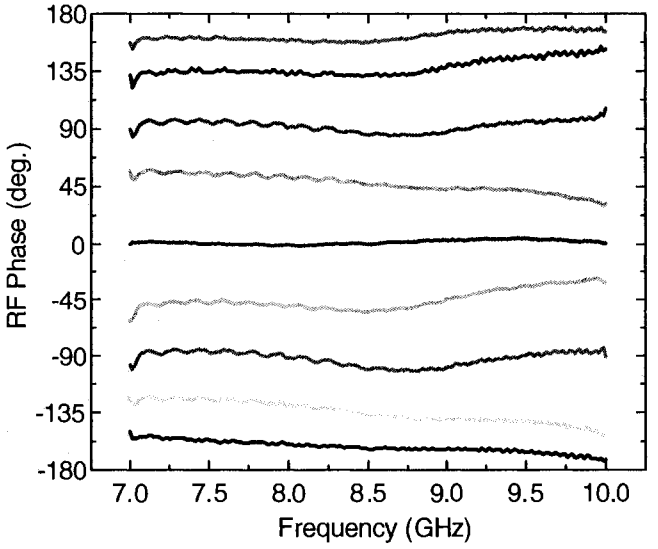

Fig. 4.3. Measured phase shift for different bias voltages. The phase shift is independent of the microwave frequency.

Then, we reconnect TLS1. The system now becomes a two-tap microwave filter with one complex coefficient. The physical separation between the two FBGs is 5.5 cm, which corresponds to a time-delay difference of 550 ps or an FSR of 1.8 GHz. To measure the frequency response, we scan the frequency of the microwave signal generated by the VNA while maintaining a constant microwave power. Fig. 4.4 shows the frequency responses of the two-tap microwave filter with the bias voltages adjusted at different values. The tunability of the frequency response is demonstrated. It is different from the

tuning of the time delay difference of a delay line filter, where the shape and the 3-dB bandwidth of the frequency response are changed. In the proposed system, since only the microwave phase is changed, the shape and the 3-dB bandwidth of the filter response remain unchanged.

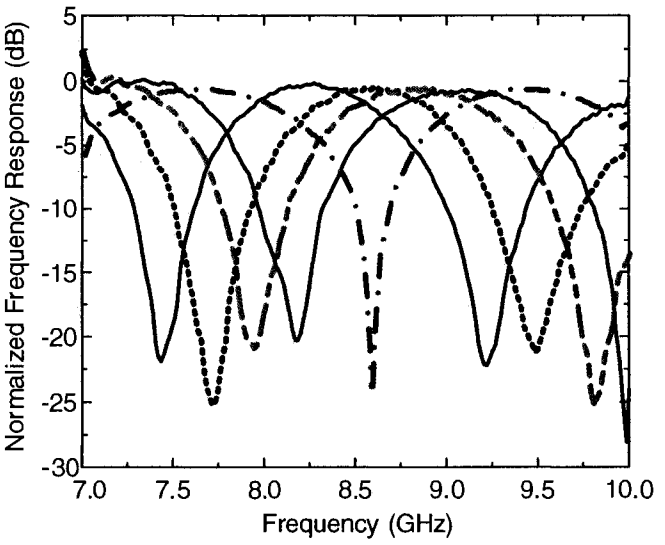

Fig. 4.4. Measured frequency response of the two-tap photonic microwave filter with one complex coefficient.

In Fig. 4.4, we can see that there are some deviations on the RF phase shifts from the ideal phase shifts at some frequencies. Accordingly, there will be some deviations from the ideal frequency response at these frequencies. This is caused by the mismatch of the fiber lengths from the outputs of the intensity

modulators to the input of the dispersive device, and the vibration of the RF cables. As a result, the shape of the frequency response will be deviated. In order to investigate the effects of the phase deviations to the filter response, we did a simulation of the frequency response corresponding to the 90° degree phase shift with and without phase deviations, as shown in Fig. 4.5. The dotted curve is the ideal frequency response without phase deviation corresponding to a phase shift of $\pi/2$, and the solid curve is the frequency response with phase deviation, corresponding to the third curve in Fig. 4.4. As can be seen, there are some small deviations on the frequency response. Since the phase deviations are not significant (less than $\sim\pi/10$), the frequency response agrees well with the ideal frequency response. If we can get rid of the mismatch of the fiber lengths from the outputs of the three intensity modulators to the input of the dispersive device, as well as the vibration of the RF cables, (which can be implemented using photonic integrated circuits technology), the accuracy control of the RF phase shift can be achieved.

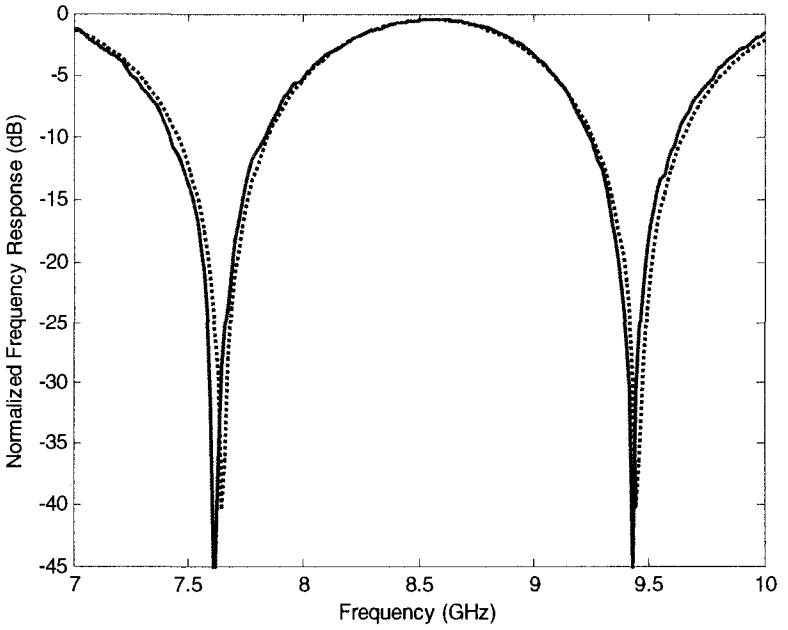

Fig. 4.5. Simulated frequency response with a phase shift of $\pi/2$. Dotted curve: ideal frequency response without phase deviation; solid curve: frequency response with phase deviation.

The phase error of the optical RF phase shifter is also attributed to the non-identical fiber lengths. The impact of the non-identical fiber lengths was evaluated. With a length difference of 2 mm, we calculated the phase shifts at different values, as shown in Fig. 4.6. It is clearly seen that the non-identical fiber lengths would contribute to the nonuniformity of the phase shifts. The nonuniformity of the fiber lengths can be compensated by using tunable optical delay line.

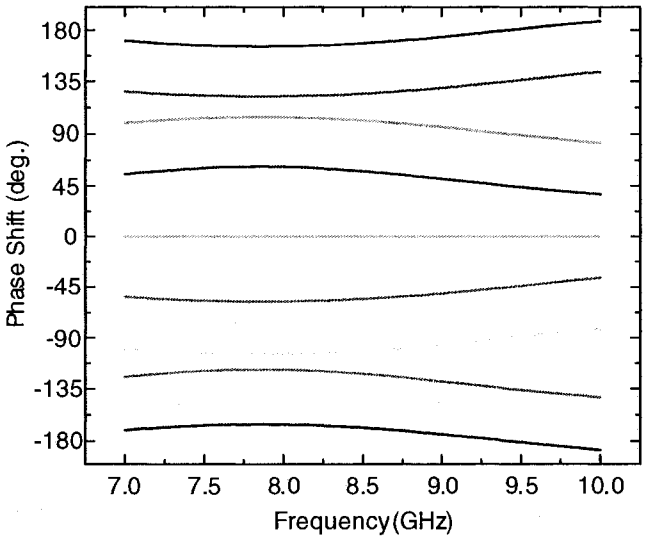

Fig. 4.6. Simulated phase shift for different bias voltages with a fiber length difference of 2 mm.

The phase error of the optical RF phase shifter is also caused by the non ideal response of the 90° hybrid RF coupler. To investigate the effect of the phase response of the 90° hybrid RF coupler to the overall response of the phase shifter, we tested the phase response of the RF coupler. Fig. 4.7 shows the phase offset between the 0° port and the 90° port of the coupler. As can be seen, there is an error (varying from -0.5 to +5 degrees) between the two ports, which will contribute to the phase shift ripple of the over all phase shift response.

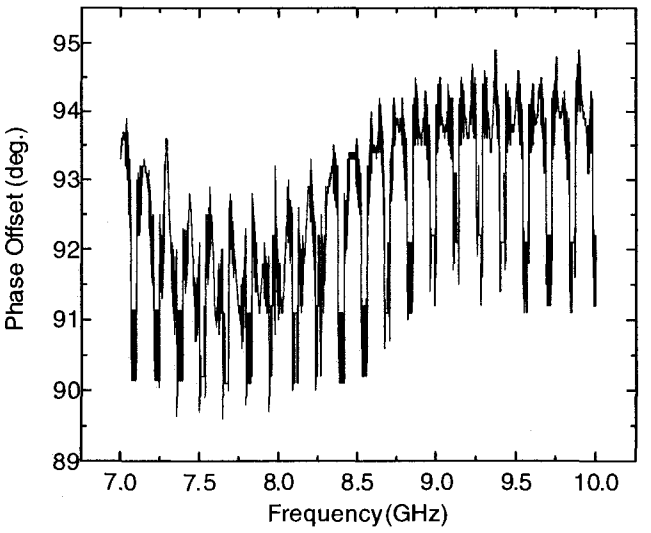

Fig. 4.7. Phase offset between the 0° port and the 90° port of the hybrid RF coupler.

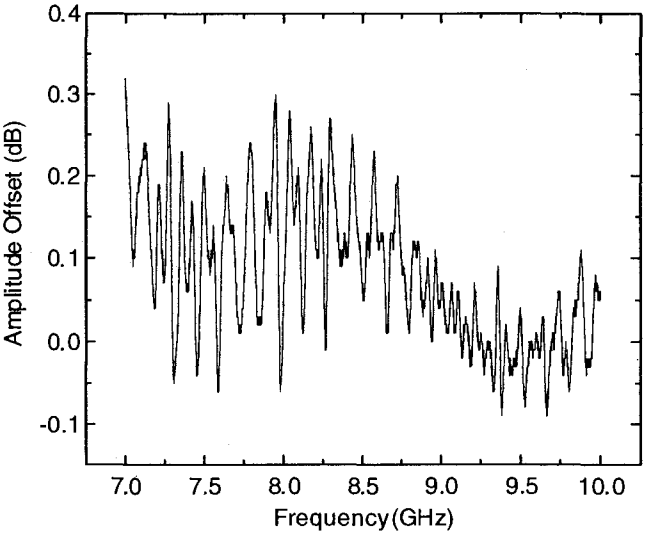

Fig. 4.8. Amplitude offset between the 0° port and the 90° port of the hybrid RF coupler.

We then tested the amplitude response of the hybrid RF coupler. Fig. 4.8 shows the amplitude offset between the 0° port and the 90° port of the coupler. As can be seen the amplitude offset between the two ports also varies with the frequency (from -0.05 dB to +0.32 dB), which will also contribute to the phase shift ripple of the over all phase shift response.

Note that the output optical intensity of IM1 will also be changed when the bias voltage V_1 is tuned to achieve the desired RF phase. In the experiment, the variation of the amplitude response due to the tuning of V_1 is compensated in two ways. One was to adjust the polarization controller (PC1) to optimize the filter response if the tuning of V_1 is small and the variation of the output optical intensity of IM1 is small; the other is to change the optical power of TLS1 if the tuning of V_1 is large. Through these two methods, the variation of amplitude response was compensated and the filter response is optimized.

We should also note that if the two FBGs are replaced by a chirped FBG, the time-delay difference between the two taps can be easily changed by simply tuning the wavelength of TLS1. This property provides an additional flexibility in the filter design.

4.3 Summary

A novel photonic microwave filter with complex coefficient was proposed and experimentally demonstrated. The complex coefficient was generated using a wideband tunable optical RF phase shifter. By simply adjusting the bias voltages applied to the two IMs, the filter response could be continuously tuned. Since the tuning was performed by adjusting the phase shift of the microwave signal, the shape of the filter response as well as the 3-dB bandwidth remained unchanged. This property is important since we can design a microwave filter that is tunable while maintaining the shape of an optimized frequency response. Another advantage of the proposed filter is that it has a very simple structure, which has the potential of being integrated using the photonic integrated circuits technology.

Chapter 5

HIGH-DYNAMIC-RANGE PHOTONIC MICROWAVE FILTER

Photonic microwave filters have attracted great attention for many years. Most of the effort in the last few years was focused on the investigation and demonstration of different architectures to realize photonic microwave filters with different functionalities [8]. The performance of photonic microwave filters should also be investigated and improved. A key factor that limits the performance of a photonic microwave filter is the spurious-free dynamic range (SFDR) [65], which is defined as the difference between the minimum signal that can be detected by the filter above the noise floor and the maximum signal that can be filtered out without distortions.

It is known that the SFDR is limited by several noise sources, including optical phase induced intensity noise, shot noise and relative-intensity noise (RIN). For a photonic microwave filter that uses independent light sources with very narrow linewidth (several tens to hundreds of kilohertz), the phase-induced intensity noise is very small and can be neglected [66]. Therefore, the dominant noise sources are the shot noise and the RIN, both are associated

with the average received optical power at the photodetector (PD). The shot noise and the RIN powers are linearly and quadratically proportional to the received optical power. Therefore, an efficient way to increase the SFDR is to reduce the average received optical power. The reduction of shot noise and the RIN to improve the dynamic range of an MPL has been extensively investigated recently, different techniques have been proposed, such as intensity-noise cancellation [67], optical carrier filtering [68], low-biasing of a Mach-Zehnder modulator (MZM) [69]-[70], coherent detection [71], class-AB modulation [72], and optical phase modulation to intensity modulation (PM-IM) conversion using an FBG-based frequency discriminator [73]. However, few efforts have been put into the investigation of techniques to improve the dynamic range of photonic microwave filters.

In this chapter, we propose a technique to improve the dynamic range of a photonic microwave bandpass filter. The photonic microwave bandpass filter is implemented based on phase modulation to intensity modulation (PM-IM) conversion using fiber Bragg gratings (FBGs) serving as frequency discriminators, with the optical carriers located at the left or right slopes of the FBGs, to generate positive or negative coefficients. The dynamic range of the photonic microwave bandpass filter is increased by reducing the optical-carrier-induced shot noise and relative intensity noise (RIN) at the

photodetector, by locating the optical carriers closer to the bottoms of the FBG reflection spectra. We demonstrate experimentally that the photonic microwave bandpass filter has an improvement in dynamic range of about 10 dB with this technique.

5.1 Principle

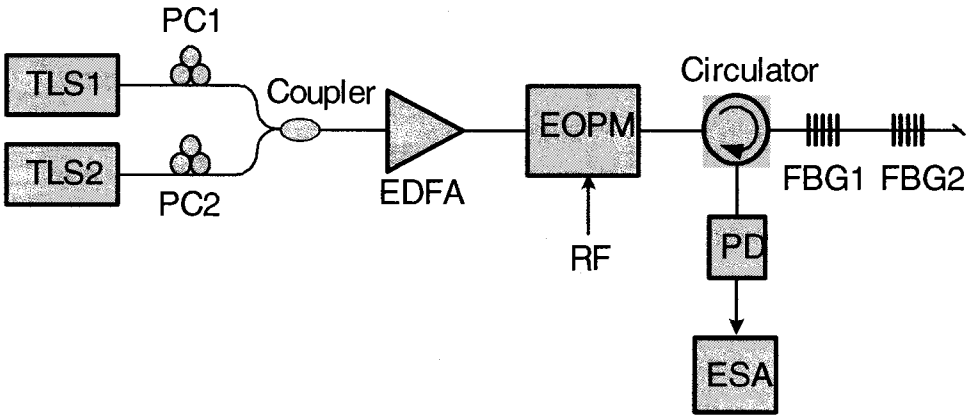

Fig. 5.1. Photonic microwave bandpass filter. TLS: tunable laser source; PC: polarization controller; EOPM: phase modulator; PD: photodetector; ESA: electrical spectrum analyzer.

The schematic diagram illustrating a two-tap photonic microwave filter is shown in Fig. 5.1. The output lightwaves from two independent tunable laser sources (TLSs) at different wavelengths are amplified by an erbium-doped fiber amplifier (EDFA), and then modulated by an RF signal to be filtered

through an electrooptic phase modulator (EOPM). Two polarization controllers (PC1 and PC2) are connected between the TLSs and the modulator to align the polarization directions of the laser beams with the principle axis of the modulator, to minimize the polarization-dependent loss. The RF signal carried by the two wavelengths is then time delayed by two cascaded FBGs, to introduce a time-delay difference.

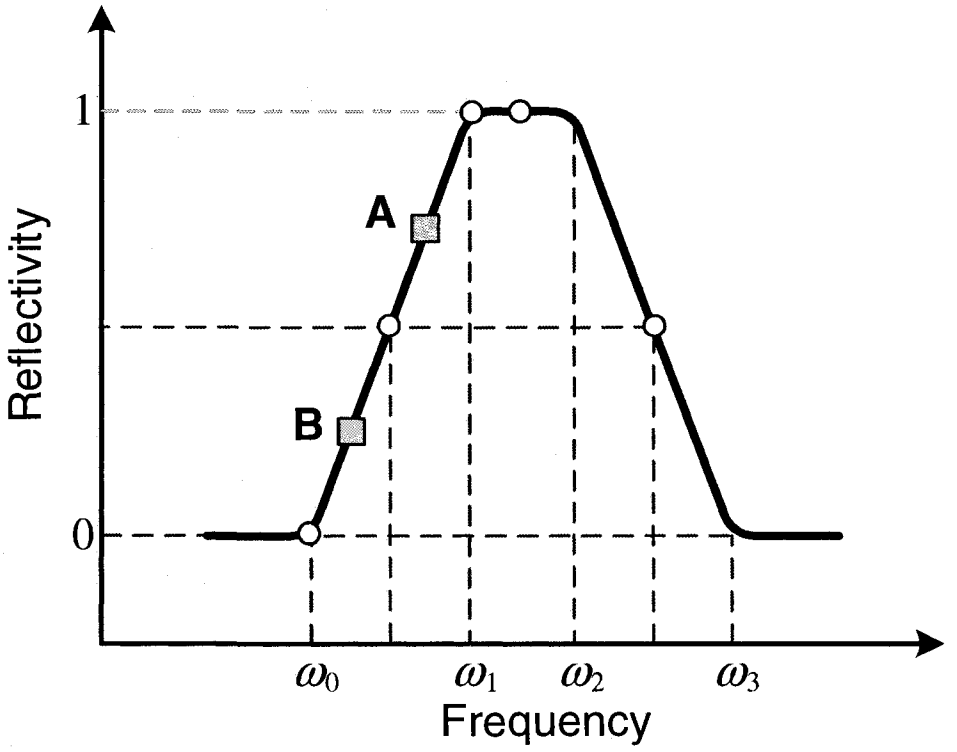

Fig. 5.2. Reflection spectrum of an ideal FBG

Fig. 5.2 shows the magnitude frequency response of an ideal FBG. For conversional photonic microwave filters, in order to get highest signal power,

each optical carrier is usually tuned to locate at the center of each FBG reflection spectrum, to get the strongest reflection. However, it is known that the shot noise at the PD exhibits a linear dependence on the average received optical power I_0, which can be expressed as

$$n_s = 2qI_0B \tag{5.1}$$

where n_s is the shot noise, q is the unit electrical charge, and B is the noise bandwidth. The RIN at the PD exhibits a quadratic dependence on the average received optical power,

$$n_{RIN} = I_0^2 B \cdot RIN \tag{5.2}$$

where $RIN = -165$ dB/Hz is the typical intensity noise of a laser source. In addition, the use of an EDFA prior to the modulator would add an amplified spontaneous emission (ASE) noise, which is resulted from the beating between the signal and the ASE. The ASE noise power spectral density is given by [70]

$$P_{ASE} = 2n_{sp}h\nu(G-1)L \tag{5.3}$$

where n_{sp} is the spontaneous emission factor, $h\nu$ is the photon energy, G is the amplifier gain, and L is the optical loss between the EDFA output and the PD.

Obviously, if the received optical power is reduced, the shot noise and the RIN at the output of the PD will be reduced. The reduction of the received optical

power can be achieved by tuning the wavelengths of the optical carriers away from the central reflection regions of the FBGs, as shown in Fig. 5.2. As the optical carrier wavelength is shifted from the top to a point closer to the bottom of the reflection spectrum, the shot noise is reduced linearly and the RIN falls quadratically. In addition, the wavelength shift will cause higher loss between the EDFA and the PD, which will also reduce the ASE noise. However, the reduction of the received optical power will also substantially decrease the RF signal power in an intensity-modulator-based system [72].

In order to increase the SFDR, it is highly desirable to lower the noise floor without sacrificing much the signal power. This can be achieved by using the configuration in Fig. 5.1, where an EOPM is used. Mathematically, when a phase-modulated optical carrier ω_c is located at the left slope, the top, or the right slope of an FBG reflection spectrum, the recovered RF signal is [74]

$$r(t) \propto \begin{cases} K^2(\omega_c - \omega_0)^2 + 2K^2(\omega_c - \omega_0)\beta_{PM} f'(t); & (\omega_0 < \omega_c < \omega_1) \\ 0; & (\omega_1 < \omega_c < \omega_2) \\ K^2(\omega_3 - \omega_c)^2 - 2K^2(\omega_3 - \omega_c)\beta_{PM} f'(t); & (\omega_2 < \omega_c < \omega_3) \end{cases} \tag{5.4}$$

where K is the slope of the FBG reflection spectrum, β_{PM} is the phase modulation index, $f'(t)$ is the first-order derivative of the modulating signal. The first and the second terms in (5.4) are respectively a DC and an AC component. Since the DC power decreases quadratically when the optical

carrier is shifted closer to the bottom of the FBG spectrum while the signal power decreases linearly, the noise power is significantly decreased while maintaining a smaller decrease in the signal power. This important characteristic enables us to choose the reflection point closer to the bottom of the FBG spectrum, to substantially reduce the optical-power-induced noises with slight sacrifice in the signal power, leading to an increased SFDR. For example, in Fig. 5.2, if the optical carrier is shifted from A to B, the optical power is reduced by nine times, while the AC power is reduced by three times. Therefore, an improvement in SFDR of 5 dB is achieved.

In addition, when the optical carrier is located at one of the two slopes of the FBG spectrum, the FBG is serving as frequency discriminator, to convert the phase modulated signal to an intensity-modulated signal.

Furthermore, for many applications, such as in a RoF system, microwave filters with bandpass functionality are highly desirable. It is seen in (5.4) that when the optical carrier is located at the positive or negative slope of the FBG spectrum, the amplitude of the recovered RF signal will have positive or negative sign, which can be directly used to generate a positive or negative coefficient in a photonic microwave bandpass filter, to achieve bandpass functionality [38] [75].

5.2 Experiment

The experimental setup based on the configuration shown in Fig. 5.1 was built. Two FBGs with central wavelengths of 1548.72 and 1549.61 nm are fabricated in hydrogen-loaded fiber. In order to investigate the improvement of the dynamic range, we first replace the EOPM in Fig. 5.1 with an electrooptic intensity modulator (EOIM), and tune the wavelengths of the TLSs to the centers of the FBG spectra. Since the optical carriers are reflected at the tops of the FBG reflection spectra, high reflecting optical powers are obtained at the PD, which lead to high noises. The optical power at the PD is measured to be 0.6 dBm. The frequency response of the filter, shown in Fig. 5.3(a), is measured using a vector network analyzer (VNA, Agilent 8364A). As can be seen it is lowpass filter with a free spectral range (FSR) of 5.05 GHz. We then investigate the dynamic range of the filter. This is done by a two-tone test by applying two RF signals with frequencies at $f_1 = 5.01\,\text{GHz}$ and $f_2 = 5.02\,\text{GHz}$ to the EOIM. Since the third-order distortions are the primary concern for most filters, we measure the third-order distortions at $2f_1 - f_2 = 5\,\text{GHz}$ and $2f_2 - f_1 = 5.03\,\text{GHz}$, as well as the noise floor (1 Hz bandwidth). The results are shown in Fig. 5.3(b). As can be seen, the noise floor is -150 dBm/Hz, and the third-order SFDR is 96.33 $dB \cdot Hz^{2/3}$.

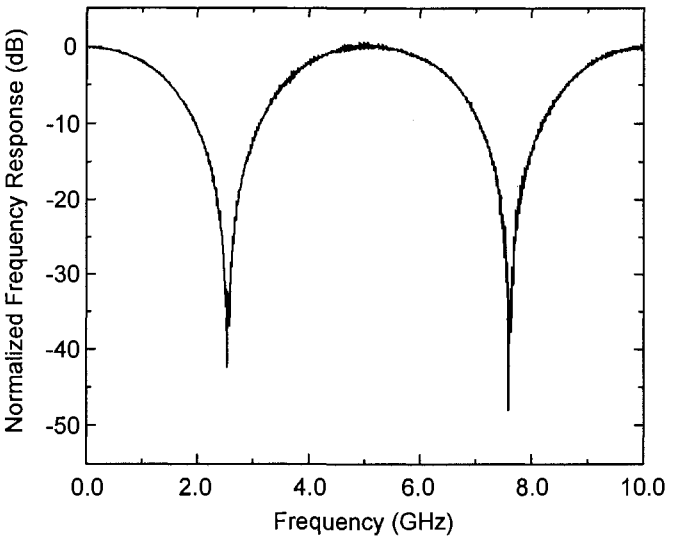

(a)

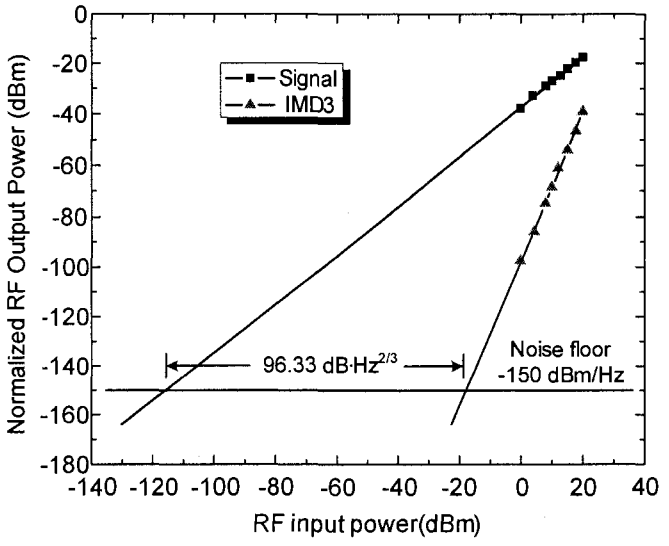

(b)

Fig. 5.3. Dynamic range of a lowpass filter with the optical carriers located at the top of the FBG reflection spectra. (a) The frequency response and (b) the dynamic range.

Then, the EOIM is replaced with an EOPM, as shown in Fig. 5.1. We tune the optical wavelengths to 1548.58 and 1549.75 nm, which are located at the left and the right reflection slopes of the FBGs, respectively. Thanks to the PM-IM conversion at the opposite slopes, a negative coefficient is generated. The filter is now a bandpass filter, with its frequency response shown in Fig. 5.4(a). The optical power at the PD is reduced to –7.8 dBm, so the optical-power-induced noises are substantially decreased, and the noise floor is reduced to -159 dBm/Hz. Again, a two-tone test is implemented, in which the input RF frequencies are chosen $f_1 = 3.51$ GHz and $f_2 = 3.52$ GHz. The third-order distortions are at $2f_1 - f_2 = 3.5$ GHz and $2f_2 - f_1 = 3.53$ GHz. The measured third-order SFDR is 106.05 $dB \cdot Hz^{2/3}$, about 10 dB dynamic range improvement is achieved.

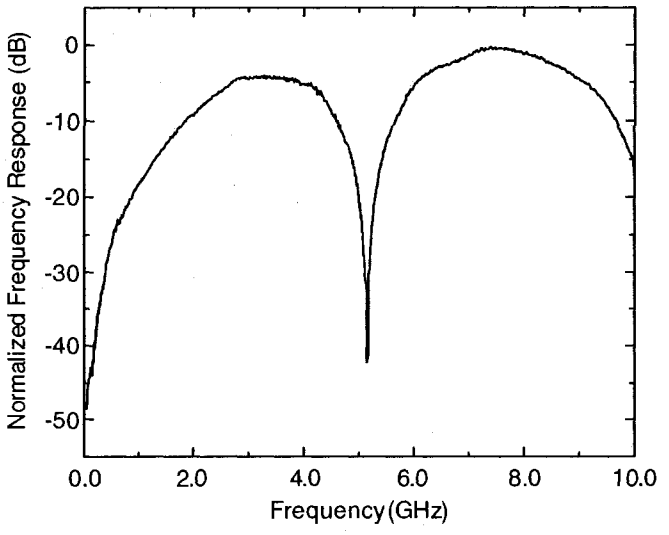

(a)

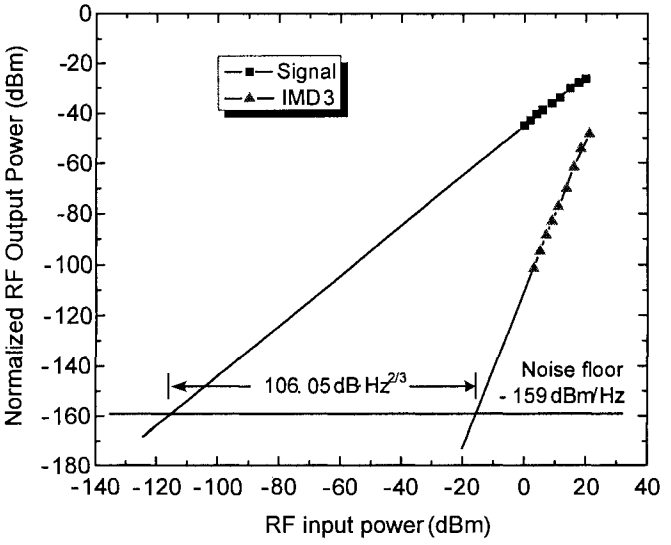

(b)

Fig. 5.4. Dynamic range of a bandpass filter with the optical carriers located at the opposite slopes of the FBG reflection spectra. (a) The frequency response and (b) the dynamic range.

5.3 Summary

In this chapter, a technique to increase the dynamic range of a photonic microwave bandpass filter was proposed and experimentally evaluated. The key of the technique was to lower the optical-carrier-induced noises, to reduce the noise floor at the output of the filter. A better dynamic range was obtained when the optical carriers were located at the lower slopes of the FBG reflection spectra. One added advantage to the technique is that by locating the

phase-modulated optical carriers at opposite slopes of the FBG reflection spectra, a microwave bandpass filter was obtained. It is believed that optimal locations must exist to make the filters to have a maximized dynamic range.

Chapter 6

CONCLUSIONS AND FUTURE WORK

6.1 Conclusions

The four objectives of this work were (1) to realize photonic microwave bandpass filter with negative coefficients based on XPolM in SOA, (2) to realize continuously tunable photonic microwave bandpass filter with negative coefficients based on PM-IM conversion in LCFBGs with opposite dispersions, (3) to realize tunable photonic microwave filter with complex coefficients based on tunable optical RF phase shifter and (4) to investigate the technique to improve the dynamic range of the photonic microwave bandpass filter. All the four objectives were achieved.

In Chapter 2, a photonic microwave bandpass filter with negative coefficients based on cross polarization modulation (XPolM) in an SOA was proposed and experimentally implemented. Thanks to the XPolM in the SOA, two microwave signals carried by two optical carriers with orthogonal polarizations were out of phase, leading to the generation of a negative

coefficient. A time delay difference between the two out-of-phase microwave signals was introduced by passing the optical microwave signals through a high birefringence (Hi-Bi) fiber. The impact of the SOA cross gain modulation (XGM) on the performance of the microwave filter was also investigated.

In Chapter 3, a continuously tunable photonic microwave bandpass filter with positive and negative coefficients using an optical phase modulator and chirped fiber Bragg gratings was proposed and experimentally demonstrated. The positive and negative coefficients were generated through optical phase-modulation to intensity-modulation (PM-IM) conversion by reflecting the phase-modulated optical carrier from linearly-chirped fiber Bragg gratings (LCFBGs) with positive and negative dispersions. The tunability was achieved by changing the wavelength of the optical carrier such that it was reflected at different physical locations in the LCFBGs.

In Chapter 4, we proposed a novel tunable microwave filter with complex coefficients using a wideband tunable optical RF phase shifter that consists of two electro-optic intensity modulators. By simply adjusting the bias voltages applied to the two intensity modulators, the filter response could be continuously tuned, and the 3-dB bandwidth and the shape of the filter response could be maintained unchanged.

Finally, a technique to improve the dynamic range of a photonic microwave bandpass filter was proposed and experimentally investigated in Chapter 5. The bandpass filter was implemented based on PM-IM conversion using FBGs serving as frequency discriminators. The dynamic range of the filter was increased by reducing the optical-carrier-induced shot noise and relative intensity noise (RIN) at the photodetector, which was realized by placing the optical carriers at the locations closer to the bottoms of the FBG reflection spectra.

6.2 Future work

First, in photonic microwave filters with complex coefficients, more work should be done to optimize the phase response of the optical RF phase shifter, which is the key device to generating the complex coefficients. As shown in Chapter 4, the phase responses of the optical RF phase shifter are not totally independent of the input RF frequency, and there are also some phase variations. This is caused by the unequal fiber lengths of the two arms, and also because of the measurement errors, including the variations of the optical fibers and the RF cables. The inequality of the fiber lengths can be compensated by using tunable optical delay line. Photonic integrated circuit

technology is a promising solution to the problem, which can reduce the phase error to less than 3° [63].

Another important issue that should be studied in the future is to further increase the dynamic range of the photonic microwave filer. As discussed in Chapter 5, the dynamic range can be increased by placing the optical carriers closer to the bottoms of the FBG reflection spectra. However, if the optical carriers are placed too close to the bottom, inter-modulation distortion will take effect. Also, if the noise floor is reduced to the noise limit of the PD, it will not reduce any more with the shift of the optical carrier. Therefore, there must be an optimal location to make the filter to have a maximized dynamic range, which needs to be thoroughly investigated.

Finally, in order to make the photonic microwave filter suitable for practical applications, more efforts should be invested to realize high-performance and low-cost multi-tap photonic microwave filters with negative and complex coefficients. Photonic integrated circuit technology may be a promising solution to this problem. The goal is to realize system-on-chip photonic microwave filters.

BIBLIOGRAPHY

[1] S. K. Mitra, *Digital signal processing: a computer based approach.* McGraw-Hill, 2006.

[2] A. Oppenheim, R. Schaffer and J. R. Buck, *Discrete-Time signal processing.* Upper Saddle River, NJ: Prentice-Hall, 1998.

[3] J. G. Proakis, and D. G. Manolakis, *Digital signal processing: principles, algorithms and applications.* Upper Saddle River, NJ: Prentice-Hall, 1996.

[4] I. C. Hunter, L. Billonet, B. Jarry, and P. Guillon, "Microwave filters — applications and technology," *IEEE Trans. Microw. Theory Tech.*, vol. 50, no. 3, pp. 794-805, Mar. 2002.

[5] K. Jackson, S. Newton, B. Moslehi, M. Tur, C. Cutler, J. Goodman, and H. J. Shaw, "Optical fiber delay-line signal processing," *IEEE Trans. Microw. Theory Tech.*, vol. MTT-33, no. 3, pp. 193-204, Mar. 1985.

[6] A. Seeds, "Microwave photonics," IEEE Trans. Micorw. Theory Tech., vol. 50, no. 3, pp. 877-887, Mar. 2002.

[7] J. Capmany, B. Ortega, D. Pastor, and S. Sales, "Discrete-time optical processing of microwave signals," *J. Lightw. Technol.*, vol. 23, no. 2, pp. 702-723, Feb. 2005.

[8] J. Capmany, B. Ortega, and D. Pastor, "A tutorial on microwave photonic filters," *J. Lightw. Technol.*, vol. 24, no. 1, pp. 201-229, Jan. 2006.

[9] K. Sasayama, M. Okuno, and K. Habara, "Coherent optical transversal filter using silica-based waveguides for high-speed signal processing," *J. Lightw. Technol.*, vol. 9, no. 10, pp. 1225-1230, Oct. 1991.

[10] F. Coppinger, C. K. Madsen, and B. Jalali, "Photonic microwave filtering using coherently coupled integrated ring resonators," *Microw. Opt. Technol. Lett.*, vol. 21, pp. 90-93, Feb. 1999.

[11] K. Wilner, A. P. Van den Heuvel, "Fiber-optic delay lines for microwave signal processing," *Proc. IEEE*, vol. 64, pp. 805-807, May 1976.

[12] E. C. Heyde and R. A. Minasian, "A solution to the synthesis problem of recirculating optical delay line filter," *IEEE Photon. Technol. Lett.*, vol. 6, pp. 833-835, Jul. 1994.

[13] J. Capmany, J. Cascon, J. L. Martin, S. Sales, D. Pastor, J. Marti, "Synthesis of fiber-optic delay line filters," *J. Lightw. Technol.*, vol. 13, pp. 2003-2012, Oct. 1995.

[14] J. Capmany, J. Martin, "Solutions to the synthesis problem of optical delay line filters," *Opt. Lett.*, vol. 20, no. 23, pp. 2438-2440, Dec. 1995.

[15] D. B. Hunter and R. Minasian, "Reflectivity tapped fiber optic transversal filter using in-fiber Bragg gratings," *Electron. Lett.*, vol. 31, pp. 1010-1012, Jun. 1995.

[16] D. B. Hunter and R. Minasian, "Microwave optical filters using in-fiber Bragg grating arrays," *IEEE Microwave and Guided Wave Lett.*, vol. 6, pp. 103-105, Feb. 1996.

[17] D. B. Hunter and R. Minasian, "Photonic signal processing of microwave signals using an active-fiber Bragg-grating-pair structure," *IEEE Trans. Microwave Theory and Technol.*, vol. MTT-45, pp. 1463-1466, Aug. 1997.

[18] J. Marti, F. Ramos and R. I. Laming, "Photonic microwave filter employing multimode optical sources and wideband chirped fiber gratings," *Electron. Lett.*, vol. 34, no. 18, pp. 1760-1761, Sept. 1998.

[19] J. Capmany, D. Pastor and B. Ortega, "New and flexible fiber-optic delay-line filters using chirped Bragg gratings and laser arrays," *IEEE Trans. Microwave Theory and Technol.*, vol. 47, no. 7, pp. 1321-1326, Jul. 1999.

[20] J. Marti, V. Polo, F. Ramos and D. Moodie, "Photonics tunable microwave filters employing electro-absorption modulators and wideband chirped fiber gratings," *Electron. Lett.*, vol. 35, no. 4, pp. 305-306, Feb. 1999.

[21] G. Yu, W. Zhang, and J. A. R. Williams, "High-performance microwave transversal filter using fiber Bragg grating arrays," *IEEE Photon. Technol. Lett.*, vol. 12, no. 9, pp. 1183-1185, Sept. 2000.

[22] D. Pastor, J. Capmany, and B. Ortega, "Broad-band tunable microwave transversal notch filter based on tunable uniform fiber Bragg gratings as slicing filters," *IEEE Photon. Technol. Lett.*, vol. 13, no. 7, pp. 726-728, Jul. 2001.

[23] W. Zhang, J. A. R. Williams, and I. Bennion, "Polarization synthesized optical transversal filter employing high birefringence fiber gratings," *IEEE Photon. Technol. Lett.*, vol. 13, no. 5, pp. 523-525, May. 2001.

[24] D. Pastor, J. Capmany and B. Ortega, "Experimental demonstration of parallel fiber-optic-based RF filtering using WDM techniques," *IEEE Photon. Technol. Lett.*, vol. 12, no. 1, pp. 77-78, Jan. 2000.

[25] V. Polo, B. Vidal, J. L. Corral, and J. Marti, "Novel tunable photonics microwave filter based on laser arrays and NxN AWG-based delay lines," *IEEE Photon. Technol. Lett.*, vol. 15, no. 4, pp. 584-586, Apr. 2003.

[26] T. A. Cusick, S. Iezekiel, R.E Miles, S. Sales, J. Capmany, "Synthesis of all-optical microwave filters using Mach-Zehnder lattices," *IEEE Trans. Microwave Theory and Technol.*, vol. 45, pp. 1458-1462, Aug. 1997.

[27] D. Norton, S. Johns, C. Keefer and R. Soref, "Tunable microwave filtering using high dispersion fiber time delays," *IEEE Photon. Technol. Lett.*, vol. 6, pp. 831-832, Jul. 1994.

[28] K. H. Lee, W. Y. Choi, S. Choi and K. Oh, "A novel tunable fiber-optic microwave filter using multimode DCF," *IEEE Photon. Technol. Lett.*, vol. 15, no. 7, Jul. 2003.

[29] S. Sales, J. Capmany, J. Marti, and D. Pastor, "Experimental demonstration of fiber-optic delay line filters with negative coefficients," *Electron. Lett.*, vol. 31, pp. 1095-1096, Jul. 1995.

[30] F. Coppinger, S. Yegnanarayanan, P. D. Trinh, and B. Jalali, "All-optical RF filter using amplitude inversion in a semiconductor optical amplifier," *IEEE Trans. Microw. Theory Tech.*, vol. 45, no. 8, pp. 1473-1477, Aug. 1997.

[31] T. Mukai, K. Inoue, and T. Saitoh, "Homogeneous gain saturation in 1.5 m InGaAsP traveling-wave semiconductor laser amplifiers," *Appl. Phys. Lett.*, vol. 28, pp. 381-383, 1987.

[32] X. Wang and K. T. Chan, "Tunable all-optical incoherent bipolar delay-line filter using injection-locked Fabry-Paret laser and fiber Bragg gratings," *Electron. Lett.*, vol. 36, pp. 2001-2002, Dec. 2000.

[33] S. Li, K. S. Chiang, W. A. Gambling, Y. Liu, L. Zhang, and I. Bennion, "A novel tunable all-optical incoherent negative-tap fiber-optical transversal filter based on a DFB laser diode and fiber Bragg gratings," *IEEE Photon. Technol. Lett.*, vol. 12, no. 9, pp. 1207-1209, Sep. 2000.

[34] S. Li, K. T. Chan, and C. Lou, "Wavelength switching of picosecond pulses in a self-seeded Fabry-Perot semiconductor laser with external fiber Bragg grating cavities by optical injection," *IEEE Photon. Technol. Lett.*, vol. 10, pp. 1094-1096, Aug. 1998.

[35] J. Capmany, D. Pastor, A. Martinez, B. Ortega, and S. Sales, "Microwave photonics filter with negative coefficients based on phase inversion in an electro-optic modulator," *Opt. Lett.*, vol. 28, pp. 1415-1417, Aug. 2003.

[36] J. Mora, M. V. Andres, J. L. Cruz, B. Ortega, J. Capmany, D. Pastor, and S. Sales, "Tunable all-optical negative multitap microwave filters based on uniform fiber Bragg gratings," *Opt. Lett.*, vol. 28, pp. 1308-1310, Aug. 2003.

[37] F. Zeng, J. Wang, and J. P. Yao, "All-optical microwave bandpass filter with negative coefficients based on a phase modulator and linearly chirped fiber Bragg gratings," *Opt. Lett.*, vol. 30, no. 17, pp. 2203-2205, Sep. 2005.

[38] J. Wang, F. Zeng, and J. P. Yao, "All-optical microwave bandpass filter with negative coefficients based on PM-IM conversion," *IEEE Photon. Technol. Lett.*, vol. 17, no.10, pp. 2176- 2178, Oct. 2005.

[39] J. P. Yao and Q. Wang, "Photonic microwave bandpass filter with negative coefficients using a polarization modulator," *IEEE Photon. Technol. Lett.*, vol. 19, no. 9, pp. 644-646, May 2007.

[40] N. You, and R. A. Minasian, "A novel tunable microwave optical notch filter," *IEEE Trans. Microw. Theory Tech.*, vol. 49, no. 10, pt. 2, pp. 2002-2005, Oct. 2001.

[41] A. Loayssa, J. Capmany, M. Sagues, and J. Mora, "Demonstration of incoherent microwave photonic filters with all-optical complex coefficients," *IEEE Photon. Technol. Lett.*, vol. 18, no. 16, pp. 1744-1746, Aug. 2006.

[42] W. Zhang, J. A. R. Williams, and I. Bennion, "Optical fiber delay line filter free of limitation imposed by optical coherence," *Electron. Lett.*, vol. 35, no. 24, pp. 2133-2134, Nov. 1999.

[43] C. K. Oh, T. Y. Kim, S. H. Baek, and C. S. Park, "Photonic microwave notch filter using cross polarization modulation in highly nonlinear fiber and polarization-dependent optical delay in high birefringence fiber," *Opt. Express*, vol. 14, no. 15, pp. 6628-6633, Jul. 2006.

[44] R. J. Manning, A. Antonopoulos, R. Le Roux, and A. E. Kelly, "Experimental measurement of nonlinear polarization rotation in semiconductor optical amplifiers," *Electron. Lett.*, vol. 37, pp. 229-231, Feb. 2001.

[45] L. Q. Guo, M. J. Connelly, "Signal-induced birefringence and dichroism in a tensile-strained bulk semiconductor optical amplifier and its

application to wavelength conversion," *J. Lightw. Technol.*, vol. 23, no. 12, pp. 4037-4045, Dec. 2005.

[46] F. Zeng, J. P. Yao, and S. Mihailov, "Genetic algorithm for fiber Bragg grating based all-optical microwave filter synthesis," *Opt. Eng.*, vol. 42, no. 8, pp. 2250-2256, Aug. 2003.

[47] M. Asghari, I. H. White, and R. V. Penty, "Wavelength conversion using semiconductor optical amplifiers," *J. Lightw. Technol.*, vol. 15, no. 7, pp. 1181, Jul. 1997.

[48] M. F. C. Stephens, M. Asghari, R. V. Panty, and I. H. White, "Demonstration of ultrafast all-optical wavelength conversion utilizing birefringence in semiconductor optical amplifiers," *IEEE Photon. Technol. Lett.*, vol. 9, pp. 449-451, Apr. 1997.

[49] H. Soto, D. Erasme, and G. Guekos, "Cross-polarization modulation in semiconductor optical amplifiers," *IEEE Photon. Technol. Lett.*, vol. 11, pp. 970-972, Aug. 1999.

[50] Y. Liu, M. T. Hill, E. Tangdiongga, H. de Waardt, N. Calabretta, G. D. Khoe, and H. J. S. Dorren, "Wavelength conversion using nonlinear polarization rotation in a single semiconductor optical amplifier," *IEEE Photon. Technol. Lett.*, vol. 15, no. 1, pp. 90-92, Jan. 2003.

[51] X. P. Mao, R. W. Tkach, A. R. Chraplyvy, R. M. Jopson, and R. M. Derosier, "Stimulated Brillouin threshold dependence on fiber type and uniformity," *IEEE Photon. Technol. Lett.*, vol. 4, no. 1, Jan. 1992.

[52] J. Hansryd, F. Dross, M. Westlund, P. A. Andrekson, and S. N. Knudsen, "Increase of the SBS threshold in a short highly nonlinear fiber by applying a temperature distribution," *J. Lightw. Technol.*, vol. 19, no. 11, pp. 1691-1697, Nov. 2001.

[53] F. Zeng and J. P. Yao, "All-optical bandpass microwave filter based on an electro-optical phase modulator," *Opt. Express*, vol. 12, no. 16, pp. 3814-3819, Aug. 2004.

[54] J. Wang, F. Zeng, and J. P. Yao, "All-optical microwave bandpass filters implemented in a radio-over-fiber link," *IEEE Photon. Technol. Lett.*, vol. 17, no. 8, pp. 1737-1739, Aug. 2005.

[55] J. E. Bowers, S. A. Newton, and H. J. Shaw, "Fiber optic variable delay lines," *Electron. Lett.*, vol. 18, no. 23, pp. 999-1000, Nov. 1982.

[56] F. Coppinger, S. Yegnanarayanan, P. D. Trinh, B. Jalali, and I. L. Newberg, "Nonrecursive tunable photonic filter using wavelength-selective true time delay," *IEEE Photon. Technol. Lett.*, vol. 8, no. 9, pp. 1214-1216, Sep. 1996.

[57] D. B. Hunter, R. A. Minasian, and P. A. Krug, "Tunable optical transversal filter based on chirped gratings," *Electron. Lett.*, vol. 31, no. 25, pp. 2205-2207, Dec. 1995.

[58] M. Delgado-Pinar, J. Mora, A. Diez, M. V. Andres, B. Ortega, and J. Capmany, "Tunable and reconfigurable microwave filter by use of a Bragg-grating-based acousto-optic superlattice modulator," *Opt. Lett.*, vol. 30, no. 1, pp. 8-10, Jan. 2005.

[59] J. Mora, B. Ortega, M. V. Andres, J. Capmany, J. L. Cruz, D. Pastor, and S. Sales, "Tunable dispersion device based on a tapered fiber Bragg grating and nonuniform magnetic fields," *IEEE Photon. Technol. Lett.*, vol. 15, no. 7, pp. 951-953, Jul. 2003.

[60] F. Zeng and J. P. Yao, "Investigation of phase-modulation-based all-optical bandpass microwave filter," *J. Lightw. Technol.*, vol. 23, no. 4, pp. 1721-1728, Apr. 2005.

[61] F. Zeng, "All-optical microwave signal processing based on optical phase modulation," Ph. D. Thesis, University of Ottawa, 2006.

[62] Y. Yan and J. P. Yao "A tunable photonic microwave filter with complex coefficient using an optical RF phase shifter," *IEEE Photon. Technol. Lett.*, to appear.

[63] J. F. Coward, T. K. Yee, C. H. Chalfant, and P. H. Chang, "A photonic integrated-optic RF phase shifter for phased array antenna beam-forming

applications," *J. Lightw. Technol.*, vol. 11, no. 12, pp. 2201-2205, Dec. 1993.

[64] S. T. Winnall, A. C. Lindsay, and G. A. Knight, "A wide-band microwave photonic phase and frequency shifter," *IEEE Trans. Microw. Theory Tech.*, vol. 45, no. 6, pp. 1003-1006, Jun. 1997.

[65] J. H. Schaffner and W. B. Bridges, "Intermodulation distortion in high dynamic range microwave fiber-optic links with linearized modulators," *J. Lightw. Technol.*, vol. 11, no. 1, pp. 3-6, Jan. 1993.

[66] S. Yamamoto, N. Edagawa, H. Taga, Y. Yoshida, and H. Wakabayashi, "Analysis of laser phase noise to intensity noise conversion by chromatic dispersion in intensity modulation and direct detection optical-fiber transmission," *J. Lightw. Technol.*, vol. 8, no. 11, pp. 1716-1722, Nov. 1990.

[67] S. Mathai, F. Cappelluti, T. Jung, D. Novak, R. B. Waterhouse, D. Siveco, A. Y. Cho, G. Ghione, and M. C. Wu, "Experimental demonstration of a balanced electroabsorption modulated microwave photonic link," *IEEE Trans. Microw. Theory Tech.*, vol. 49, no. 10, pp. 1956-1961, Oct. 2001.

[68] R. D. Esman and K. J. Williams, "Wideband efficiency improvement of fiber optic systems by carrier subtraction," *IEEE Photon. Technol. Lett.*, vol. 7, no. 2, pp. 218-220, Feb. 1995.

[69] L. T. Nichols, K. J. Williams, and R. D. Esman, "Optimizing the ultrawide-band photonic link," *IEEE Trans. Microw. Theory Tech.*, vol. 47, no. 7, pp. 1194-1200, Jul. 1999.

[70] X. J. Meng and A. Karim, "Microwave photonic link with carrier suppression for increased dynamic range," *Fiber and Integrated Optics*, vol. 25, pp. 161-174, 2006.

[71] A. C. Lindsay, "An analysis of coherent carrier suppression for photonic microwave links," *IEEE Trans. Microw. Theory Tech.*, vol. 49, no. 10, pp. 1956-1961, Oct. 2001.

[72] T. E. Darcie, A. Moye, P. F. Driessen, J. D. Bull, H. Kato, and N. A. F. Jaeger, "Noise reduction in class-AB microwave-photonic links," *IEEE MWP 2005.*

[73] J. Zhang, and T. E. Darcie, "Low-biased microwave-photonic link using optical frequency or phase modulation and fiber-Bragg-grating discriminator," *OFC/NFOEC 2006*, Anaheim, CA, Paper OWG1, Mar. 2006.

[74] Q. Wang and J. P. Yao, "An electrically switchable optical Ultra-Wideband pulse generator," *J. Lightw. Technol.*, to appear.

[75] F. Zeng and J. P. Yao, "Frequency domain analysis of fiber Bragg grating based phase modulation to intensity modulation conversion," *Proc. of SPIE*, vol. 5971, 59712B, Sep. 2005.

LIST OF ACRONYMS

A

ASE	Amplified Spontaneous Emission
AWG	Arrayed Wave Guide

B

BIBO	Bounded Input Bounded Output
BPF	Bandpass Filter

C

CW	Continuous Wave

D

DFB	Distributed Feedback

E

ECM	Electronic Counter Measures
EDFA	Erbium Doped Fiber Amplifier
EMI	Electromagnetic Interference
E/O	Electrical-to-Optical
EOIM	Electro-Optic Intensity Modulator
EOPM	Electro-Optic Phase Modulator
ESM	Electronic Support Measures

F

FBG	Fiber Bragg Grating
FIR	Finite Impulse Response
FP	Fabry-Perot
FSR	Free Spectral Range

H

Hi-Bi	High Birefringence
HNLF	Highly Nonlinear Fiber

I

IM	Intensity Modulation

L

LCFBG	Linearly Chirped Fiber Bragg Grating
LD	Laser Diode
LED	Light Emission Diode

M

MPL	Microwave-photonic Link
MZM	Mach-Zehnder Modulator

O

O/E	Optical-to-electrical
OSA	Optical Spectrum Analyzer

P

PBS	Polarization Beam Splitter
PC	Polarization Controller
PD	Photodetector
PM	Phase Modulation

PM-IM Phase-modulation to Intensity-modulation
PMF Polarization Maintaining Fiber
PolM Polarization Modulator

R

RF Radio Frequency
RIN Relative Intensity Noise
RoF Radio-over-fiber

S

SBS Stimulated Brillouin Scattering
SFDR Spurious-free Dynamic Range
SLED Superluminescent Light Emitting Diode
SOA Semiconductor Optical Amplifier
SSB Single Side Band

T

TE Transverse Electric
TL Tunable Laser
TLS Tunable Laser Source
TM Transverse Magnetic

U

UFBG Uniform Fiber Bragg Grating

V

VNA Vector Network Analyzer

X

XGM Cross Gain Modulation
XPolM Cross Polarization Modulation